

PAPER: Quantum statistical physics, condensed matter, integrable systems

Yang–Baxter integrable dimers on a strip

Paul A Pearce^{1,2}, Jørgen Rasmussen²
and Alessandra Vittorini-Orgeas¹

¹ School of Mathematics and Statistics, University of Melbourne, Parkville, Victoria 3010, Australia

² School of Mathematics and Physics, University of Queensland, St Lucia, Brisbane, Queensland 4072, Australia

E-mail: papearce@unimelb.edu.au, j.rasmussen@uq.edu.au
and alessandra.vittorini@unimelb.edu.au

Received 12 July 2019

Accepted for publication 29 October 2019

Published 22 January 2020



Online at stacks.iop.org/JSTAT/2020/013107
<https://doi.org/10.1088/1742-5468/ab54bd>

Abstract. The dimer model on a strip is considered as a Yang–Baxter integrable six vertex model at the free-fermion point with crossing parameter $\lambda = \frac{\pi}{2}$ and quantum group invariant boundary conditions. A one-to-many mapping of vertex onto dimer configurations allows for the solution of the free-fermion model to be applied to the anisotropic dimer model on a square lattice where the dimers are rotated by 45° compared to their usual orientation. In a suitable gauge, the dimer model is described by the Temperley–Lieb algebra with loop fugacity $\beta = 2 \cos \lambda = 0$. It follows that the model is exactly solvable in geometries of arbitrary finite size. We establish and solve transfer matrix inversion identities on the strip with arbitrary finite width N . In the continuum scaling limit, in sectors with magnetization S_z , we obtain the conformal weights $\Delta_s = ((2 - s)^2 - 1)/8$ where $s = |S_z| + 1 = 1, 2, 3, \dots$. We further show that the corresponding finitized characters $\chi_s^{(N)}(q)$ decompose into sums of q -Narayana numbers or, equivalently, skew q -binomials. In the particle representation, the local face tile operators give a representation of the fermion algebra and the fermion particle trajectories play the role of nonlocal degrees of freedom. We argue that, in the continuum scaling limit, there exist nontrivial Jordan blocks of rank 2 in the Virasoro dilatation operator L_0 . This confirms that, with quantum group invariant boundary conditions, the dimer model gives rise to a *logarithmic* conformal field theory with central charge $c = -2$, minimal conformal weight $\Delta_{\min} = -\frac{1}{8}$ and effective central charge $c_{\text{eff}} = 1$.

J. Stat. Mech. (2020) 013107

Our analysis of the structure of the ensuing rank 2 modules indicates that the familiar staggered $c = -2$ modules appear as submodules.

Keywords: dimers, conformal field theory, algebraic structures of integrable models, solvable lattice models

Contents

1. Introduction	3
2. Dimers as a free-fermion six vertex model	4
2.1. Face tiles and equivalence of vertex, particle and dimer representations.....	4
2.2. Free-fermion and Temperley–Lieb algebras.....	7
2.2.1. Free-fermion algebra.....	7
2.2.2. Temperley–Lieb algebra.....	8
3. Six vertex model on the strip	8
3.1. Local relations.....	9
3.1.1. Face operators, symmetries and face weights.....	9
3.1.2. Inversion relations.....	11
3.1.3. Yang–Baxter equations.....	12
3.1.4. Boundary Yang–Baxter equations.....	13
3.2. Commuting double row transfer matrices.....	14
3.2.1. Sectors and quantum numbers.....	14
3.2.2. Diagrammatic proof of commutation.....	15
4. Solution of dimers on a strip and finite-size spectra	17
4.1. Inversion identities on the strip.....	17
4.2. Combinatorial analysis of patterns of zeros.....	19
4.3. Empirical selection rules.....	22
5. Jordan decompositions and irreducible modules	25
5.1. Isotropic double row transfer matrices.....	25
5.2. Quantum Hamiltonians.....	26
5.3. Representation theory.....	27
6. Conclusion	28
Acknowledgments	30
Appendix A. Proof of inversion identities on the strip	30
Appendix B. Skew q-binomials	34
References	35

1. Introduction

The dimer model [1, 2] was solved exactly [3–6] in the early sixties. After more than 50 years, the model continues to be the subject of extensive study [7–14]. The current interest is twofold: (i) to understand the finite-size effects of boundary conditions and steric effects [15–17] under the influence of infinitely repulsive hard-core local interactions and (ii) to understand the conformal description of the model in the continuum scaling limit. Traditionally, it is asserted that the dimer model is described [18] by a $c = 1$ Gaussian free field. But without full access to the various sectors and boundary conditions on the strip, it is difficult to distinguish between a $c = 1$ theory and a $c_{\text{eff}} = 1$ theory and a number of authors [8, 9] have suggested that the model is described by a *logarithmic* conformal field theory (CFT) with $c = -2$.

Recently, the dimer model was shown [19] to be Yang–Baxter integrable [20] by mapping [17, 21, 22] it onto the free-fermion six vertex model [23–27]. Notably, this maps six vertex configurations onto dimer configurations where the dimers are rotated by 45° , as shown in figures 2, 4 and 5, compared to their usual orientation parallel to the bonds of the square lattice. This technique combined with inversion identities [20, 28, 29] enables the model to be solved exactly for finite lattices with various boundary conditions and topologies. The conformal properties can therefore be readily extracted from the finite-size scaling behaviour. On this basis, it was argued in [19] that the dimer model is best described as a logarithmic CFT with effective central charge $c_{\text{eff}} = 1$ but central charge $c = -2$, in agreement with the findings of [8–10, 14]. The primary characterization of logarithmic CFTs is the appearance of nontrivial Jordan blocks in the Virasoro dilatation operator L_0 . Indeed, for simple dimer boundary conditions on the strip, corresponding to the $U_q(\mathfrak{sl}(2))$ -invariant XX Hamiltonian \mathcal{H} of the free-fermion six vertex model, the preliminary results of [19] indicate that \mathcal{H} admits nontrivial Jordan blocks for finite systems. Since the appearance of these blocks is stable, as the system size increases, these blocks are expected to persist for large sizes and appear in the Virasoro operator L_0 .

In this paper, we solve exactly the anisotropic square lattice dimer model with the 45° rotated orientation on the strip in sectors labelled by the magnetization S_z of the related free-fermion six vertex model. This is achieved, using Yang–Baxter integrability, by mapping the model with given boundary conditions onto a free-fermion six vertex model and solving the associated inversion identities [20, 28, 29] satisfied by the double row transfer matrices. The solution of the inversion identities allows to obtain the exact finite spectra in the various sectors. Finite-size scaling then yields the central charge and the conformal weights. In addition, combinatorial analysis of the patterns of zeros, in the complex spectral parameter plane, of the double row transfer matrix eigenvalues allows us to obtain finitized characters. We confirm the central charge $c = -2$ and the conformal weights $\Delta_s = ((2 - s)^2 - 1)/8$ with $s = 1, 2, 3, \dots$. Remarkably, although the characters are different, the conformal weights coincide with those in the first column of the infinitely extended Kac table of critical dense polymers [30–35], as shown in figure 1.

The layout of the paper is as follows. In section 2, we recall the rotated dimer model on the square lattice and review its relation to the free-fermion six vertex model. We also describe the underlying free-fermion and Temperley–Lieb algebras. In section 3,

we present the local Yang–Baxter relations of the six vertex model using the particle representation of the planar algebra and establish the commutation of the double row transfer matrices. In section 4, we specialise to the dimer model and solve the associated inversion identities on the strip for the finite size spectra. This involves the combinatorial analysis of the patterns of zeros of the eigenvalues and the empirical determination of selection rules to fix the eigenvalue degeneracies which are not fixed by the functional equations alone. Jordan decompositions of the isotropic double row transfer matrices and their quantum Hamiltonians, for some small system sizes, are presented in section 5 to reveal the existence of nontrivial Jordan blocks of rank 2. In the continuum scaling limit, the Hamiltonian gives rise to the Virasoro dilatation operator L_0 . Since the indications are that these Jordan blocks persist in the continuum scaling limit, we are led to conclude that the CFT describing the dimer model is logarithmic. We also analyse the structure of the ensuing rank 2 modules and determine the finitized characters of their irreducible sub-quotients. We finish with some concluding remarks in section 6, comparing dimers with critical dense polymers. Details of the proof of the inversion identities and the properties of the skew q -binomials appearing in the selection rules are relegated to Appendices.

2. Dimers as a free-fermion six vertex model

2.1. Face tiles and equivalence of vertex, particle and dimer representations

A mapping between the free-fermion six vertex model and dimer configurations was given in [19]. The allowed six vertex (arrow conserving) face configurations and the equivalent tiles in the particle (even and odd rows) and dimer [17] representations are shown in figure 2. The vertex (arrow) degrees of freedom $\sigma_j = \pm 1$ and the particle occupation numbers $a_j = \frac{1}{2}(1 - \sigma_j) = 0, 1$ live on the medial lattice. The Boltzmann weights of the six vertex tiles are

$$a(u) = \rho \frac{\sin(\lambda - u)}{\sin \lambda}, \quad b(u) = \rho \frac{\sin u}{\sin \lambda}, \quad c_1(u) = \rho g, \quad c_2(u) = \frac{\rho}{g}, \quad \lambda \in (0, \pi), \quad \rho \in \mathbb{R}. \quad (2.1)$$

The spectral parameter u plays the role of spatial anisotropy with $u = \frac{\lambda}{2}$ being the isotropic point. Geometrically [36], varying u effectively distorts a square tile into a rhombus with an opening anisotropy angle $\vartheta = \frac{\pi u}{\lambda}$. The arbitrary parameter ρ is an overall normalization. Assuming boundary conditions such that there are an equal number of sources and sinks of horizontal arrows (vertices c_1 and c_2) along any row, the transfer matrix entries are all independent of the gauge factor g which may depend on u .

At the free-fermion point ($\lambda = \frac{\pi}{2}$), the six vertex face weights reduce to

$$a(u) = \rho \cos u, \quad b(u) = \rho \sin u, \quad c_1(u) = \rho g, \quad c_2(u) = \frac{\rho}{g}, \quad \rho \in \mathbb{R}. \quad (2.2)$$

These weights satisfy the free-fermion condition

s	\vdots	\vdots	\vdots	\vdots	\vdots	\vdots	\ddots
10	$\frac{63}{8}$	$\frac{35}{8}$	$\frac{15}{8}$	$\frac{3}{8}$	$-\frac{1}{8}$	$\frac{3}{8}$	\dots
9	6	3	1	0	0	1	\dots
8	$\frac{35}{8}$	$\frac{15}{8}$	$\frac{3}{8}$	$-\frac{1}{8}$	$\frac{3}{8}$	$\frac{15}{8}$	\dots
7	3	1	0	0	1	3	\dots
6	$\frac{15}{8}$	$\frac{3}{8}$	$-\frac{1}{8}$	$\frac{3}{8}$	$\frac{15}{8}$	$\frac{35}{8}$	\dots
5	1	0	0	1	3	6	\dots
4	$\frac{3}{8}$	$-\frac{1}{8}$	$\frac{3}{8}$	$\frac{15}{8}$	$\frac{35}{8}$	$\frac{63}{8}$	\dots
3	0	0	1	3	6	10	\dots
2	$-\frac{1}{8}$	$\frac{3}{8}$	$\frac{15}{8}$	$\frac{35}{8}$	$\frac{63}{8}$	$\frac{99}{8}$	\dots
1	0	1	3	6	10	15	\dots
	1	2	3	4	5	6	r

Figure 1. Kac table of conformal weights $\Delta_{r,s}$ of critical dense polymers taken from [34]. The conformal weights of dimers coincide with the conformal weights in the first ($r = 1$) column of this Kac table. Both theories are described by CFTs with $c = -2$, although their conformal characters are different.

$$a(u)^2 + b(u)^2 = c_1(u)c_2(u). \tag{2.3}$$

As shown in section 2.2, with the special choice of gauge $g = z := e^{iu}$, the tiles give a representation of the free-fermion algebra with generators f_j, f_j^\dagger and, consequently, also a representation of the Temperley–Lieb algebra [37] with generators e_j and loop fugacity $\beta = 2 \cos \lambda = 0$. Explicitly, the face operators are

$$X_j(u) = \rho(\cos u I + \sin u e_j). \tag{2.4}$$

This Temperley–Lieb model is directly equivalent to an anisotropic dimer model as shown in figures 2, 4 and 5. A dimer weight is assigned to the unique square face which is half-covered by the dimer as shown in figure 4. The statistical weights assigned to ‘horizontal’ and ‘vertical’ dimers are

$$\zeta_h(u) = a(u) = \rho \cos u, \quad \zeta_v(u) = b(u) = \rho \sin u. \tag{2.5}$$

Setting $g = \rho$, and allowing for the facts that (i) the c_1 face has two allowed configurations and (ii) no dimer covers the c_2 face, it follows that

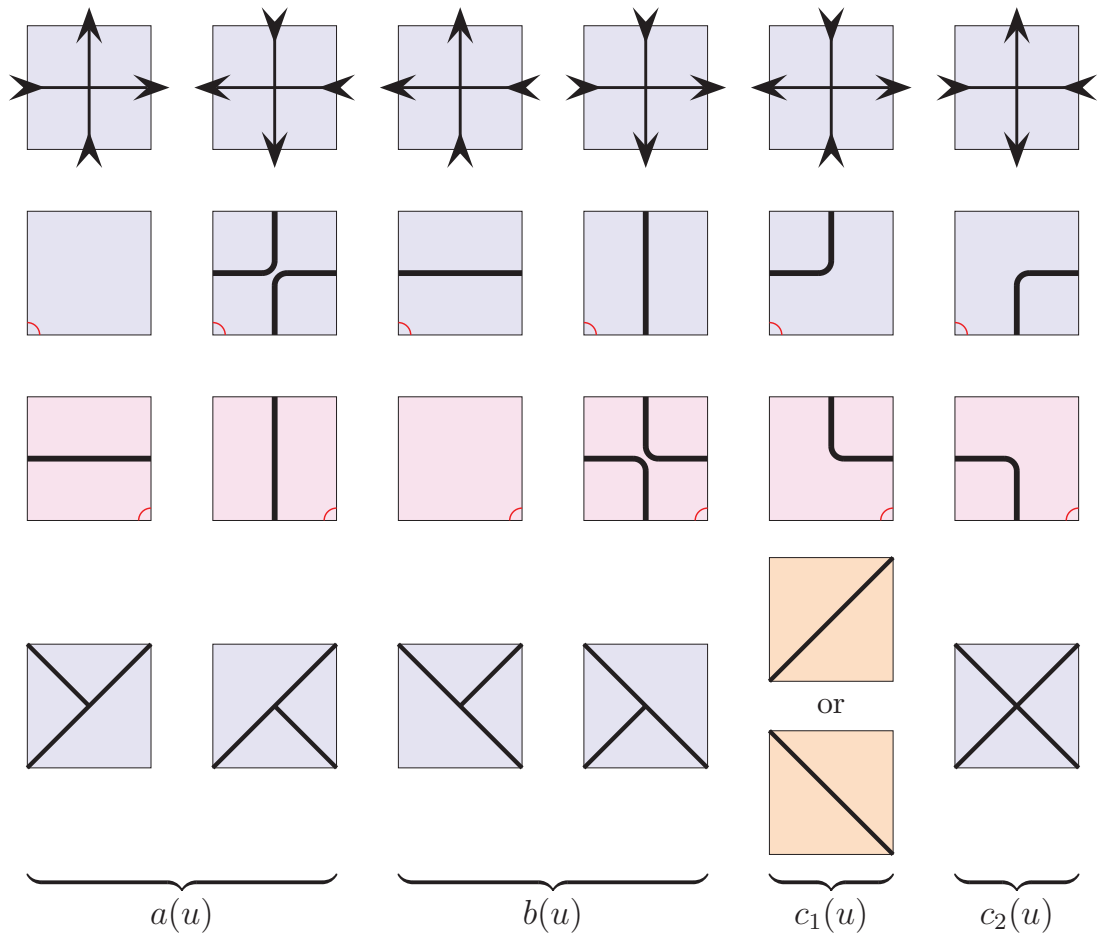


Figure 2. Equivalent face tiles of the six vertex model in the vertex, particle (even and odd rows) and dimer representations. On the strip, the odd and even rows alternate. For periodic boundary conditions, all rows are odd. The heavy particle lines are drawn whenever the arrows disagree with the reference state, as shown in figure 3. The particles move up and to the right on odd rows and up and to the left on even rows.

$$c_1(u) = \zeta_h(u)^2 + \zeta_v(u)^2 = \rho^2(\cos^2 u + \sin^2 u) = \rho^2, \quad c_2(u) = 1. \quad (2.6)$$

Additionally, fixing $\rho = \sqrt{2}$ at the isotropic point ($u = \frac{\lambda}{2} = \frac{\pi}{4}$) gives

$$a\left(\frac{\pi}{4}\right) = 1, \quad b\left(\frac{\pi}{4}\right) = 1, \quad c_1\left(\frac{\pi}{4}\right) = 2, \quad c_2\left(\frac{\pi}{4}\right) = 1. \quad (2.7)$$

It follows that, with this choice of gauge and normalization, the partition function at the isotropic point gives the correct counting of distinct dimer configurations.

In addition to the vertex and dimer representations, the six vertex free-fermion model admits a particle representation as shown in figures 2 and 5. A reference state on the strip is fixed as in figure 3. An edge of a given vertex is a segment of a particle trajectory (and has particle occupation number $a_j = 1$) if its arrow points in the opposite direction to that of the reference state. Otherwise, if the edge arrow points in the same direction as the reference state, the edge is not a segment of a particle trajectory

(and the particle occupation is $a_j = 0$). The segments of particle trajectories live on the medial lattice and are indicated with heavy lines in figure 3. The number of particles is conserved and their trajectories are non-intersecting. The particle representation is the simplest of the three representations and is convenient for coding in Mathematica [38] and for manipulations in the diagrammatic planar algebra [39] so we usually work in the particle representation. The \mathbb{Z}_2 arrow reversal symmetry of the vertex model implies a particle-hole duality in the particle representation.

2.2. Free-fermion and Temperley–Lieb algebras

In this section, we consider the free-fermion model (2.2) with $\lambda = \frac{\pi}{2}$ and set $g = z := e^{iu}$ and $\rho = 1$.

2.2.1. *Free-fermion algebra.* Regarding the elementary tiles as operators acting on an upper (zigzag) row particle configuration to produce a lower (zigzag) row particle configuration, we write them respectively as

$$E_j = n_j^{00}, n_j^{11}, f_j^\dagger f_{j+1}, f_{j+1}^\dagger f_j, n_j^{10}, n_j^{01}, \quad n_j^{00} + n_j^{11} + n_j^{10} + n_j^{01} = I. \tag{2.8}$$

The four operators n_j^{ab} are (diagonal) orthogonal projection operators which factorize into single-site orthogonal projectors corresponding to left and right half (triangular) tiles

$$n_j^{ab} = n_j^a n_{j+1}^b, \quad n_j^a n_j^b = \delta_{ab} n_j^a, \quad n_j^0 + n_j^1 = I, \quad a, b = 0, 1. \tag{2.9}$$

Here $n_j = n_j^1 = f_j^\dagger f_j$ is the number operator counting single site occupancy at position j and $n_j^0 = f_j f_j^\dagger = 1 - f_j^\dagger f_j$ is the dual number operator counting the single-site vacancies at position j . The operators f_j and f_j^\dagger are single-site particle annihilation and creation operators respectively. It follows that all of the elementary tile operators can be written as combinations of bilinears in the fermion operators f_j and f_j^\dagger . Diagrammatically, the particle hopping terms $f_j^\dagger f_{j+1}$ and $f_{j+1}^\dagger f_j$ factorize into left and right half (triangular) tiles

$$f_j^\dagger f_{j+1} = \begin{array}{c} \text{diamond} \\ \text{with diagonal line from } j \text{ to } j+1 \end{array}, \quad f_{j+1}^\dagger f_j = \begin{array}{c} \text{diamond} \\ \text{with diagonal line from } j+1 \text{ to } j \end{array} \tag{2.10}$$

so that the fermion generators are represented by half (triangular) tiles

$$f_j^\dagger = \begin{array}{c} \text{right triangle} \\ \text{with diagonal line from } j \end{array} = \begin{array}{c} \text{left triangle} \\ \text{with diagonal line to } j \end{array}, \quad f_j = \begin{array}{c} \text{left triangle} \\ \text{with diagonal line from } j \end{array} = \begin{array}{c} \text{right triangle} \\ \text{with diagonal line to } j \end{array}. \tag{2.11}$$

As defined here, the operators f_j and f_j^\dagger satisfy the mixed commutation relations

$$f_j^2 = (f_j^\dagger)^2 = 0, \quad \{f_j, f_j^\dagger\} = 1, \quad [f_j^\dagger, f_k] = [f_j^\dagger, f_k^\dagger] = [f_j, f_k] = 0, \quad j \neq k \tag{2.12}$$

so they are not, strictly speaking, fermion operators. However, it is straightforward [40] to transform by a linear transformation to new operators that are strictly fermion operators.

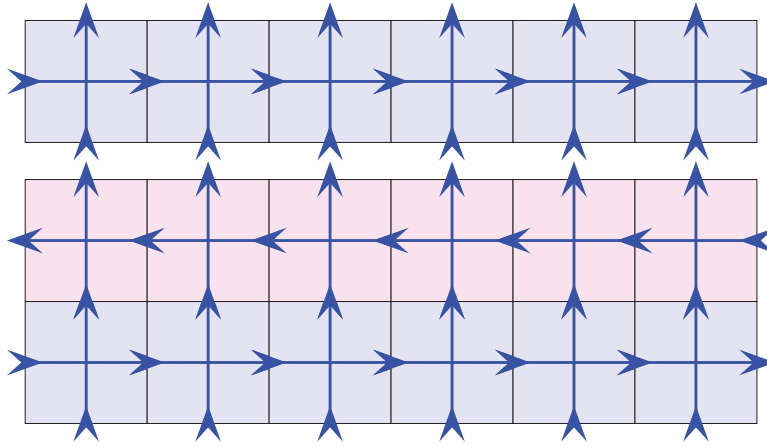


Figure 3. Reference states for the single and double row transfer matrices for mapping onto the particle representation. The reference arrows point up and to the right for the single row transfer matrices. For the double row transfer matrices, the reference arrows point up and right on odd rows and up and left on even rows.

2.2.2. *Temperley–Lieb algebra.* The Temperley–Lieb algebra is realized [41, 55] by setting $x = e^{i\lambda} = i$ and defining the generators

$$e_j = x \begin{array}{c} \diagup \\ \diagdown \end{array} + x^{-1} \begin{array}{c} \diagdown \\ \diagup \end{array} + \begin{array}{c} \diagup \\ \diagup \end{array} + \begin{array}{c} \diagdown \\ \diagdown \end{array} \tag{2.13a}$$

$$= x f_j^\dagger f_j (1 - f_{j+1}^\dagger f_{j+1}) + x^{-1} (1 - f_j^\dagger f_j) f_{j+1}^\dagger f_{j+1} + f_j^\dagger f_{j+1} + f_{j+1}^\dagger f_j \tag{2.13b}$$

$$= x f_j^\dagger f_j + x^{-1} f_{j+1}^\dagger f_{j+1} + f_j^\dagger f_{j+1} + f_{j+1}^\dagger f_j. \tag{2.13c}$$

The quartic (interacting) terms vanish, since $\beta = x + x^{-1} = 0$, leaving bilinears in fermion operators. Using the planar algebra [39] of tiles, it readily follows that these operators yield a representation of the Temperley–Lieb algebra

$$e_j^2 = \beta e_j = 0, \quad e_j e_{j\pm 1} e_j = e_j, \quad \beta = 2 \cos \lambda = x + x^{-1} = 0. \tag{2.14}$$

Equivalently this follows, purely from fermionic algebra, by writing the generators in terms of the fermionic operators f_j and f_j^\dagger as in (2.13c).

3. Six vertex model on the strip

The commuting double row transfer matrices of the six vertex model were constructed algebraically by Sklyanin [42]. In this section, we develop a diagrammatic construction of the commuting double row transfer matrices of the six vertex model by generalizing the methods of [43] and using planar algebras [39].

3.1. Local relations

We describe the local relations satisfied by the six vertex face operators in the planar and linear algebra settings. Because it has local degrees of freedom, in the form of particle occupation numbers, the planar algebra of the six vertex model just involves local tensor contractions of the indices giving the particle numbers. By fixing the planar algebra operators to act in an arbitrary fixed direction, the local relations presented in this section are easily established concretely using matrix representations (for example in Mathematica [38]). Alternatively, a local relation can be established diagrammatically directly in the planar algebra setting. It then follows that the local relation holds for all matrix representations and for all choices of the direction of action.

3.1.1. Face operators, symmetries and face weights. As elements of a planar algebra, the face operators of the six vertex model in the particle representation decompose [44] into a sum of contributions from six elementary tiles

$$\langle u, g \rangle = s_1(-u) \left(\text{tile}_1 + \text{tile}_2 \right) + s_0(u) \left(\text{tile}_3 + \text{tile}_4 \right) + g \text{tile}_5 + g^{-1} \text{tile}_6 \quad (3.1)$$

where $s_k(u) = \frac{\sin(u+k\lambda)}{\sin \lambda}$ and g is a gauge factor. Multiplication of the tiles in the planar algebra is given [19, 44] by local tensor contraction of indices $a, b, c, d, \dots = 0, 1$ specifying the particle occupation numbers on the centers of the tile edges. As orientated in (3.1), the face operators are invariant under reflection about the horizontal diagonal and not invariant (for $g \neq 1$) under reflection about the vertical diagonal. Rotating the face operator by 90° gives

$$\langle u, g \rangle = s_1(-u) \left(\text{tile}_1 + \text{tile}_2 \right) + s_0(u) \left(\text{tile}_3 + \text{tile}_4 \right) + g \text{tile}_5 + g^{-1} \text{tile}_6 \quad (3.2)$$

Further rotations by 90° give

$$\langle u, g \rangle = \langle u, g^{-1} \rangle, \quad \langle u, g \rangle = \langle u, g^{-1} \rangle \quad (3.3)$$

Only the occupation numbers $a, b, c, d = 0, 1$ of the edges are important. The colors of the face operators (indicating their relative orientation) and the internal particle trajectories are just for easy visual identification so that

$$\text{tile}_1 \equiv \text{tile}_2 \equiv \text{tile}_3 \quad (3.4)$$

Usually, we work in the fixed gauge $g = z := e^{iu}$ with $x = e^{i\lambda}$ and set

$$\langle u \rangle = \langle u, z \rangle \quad (3.5)$$

Using this gauge, gives

$$\langle u \rangle = s_1(-u) \langle 0 \rangle + s_0(u) \langle \lambda \rangle \quad (3.6)$$

J. Stat. Mech. (2020) 013107

where the generators of the planar Temperley–Lieb algebra are

$$\begin{array}{c} \text{diamond with } 0 \text{ at bottom-left} \\ = \text{yellow diamond} + \text{yellow diamond with arc on right} + \text{yellow diamond with arc on left} + \text{yellow diamond with arc on top} \end{array} \quad (3.7a)$$

$$\begin{array}{c} \text{diamond with } \lambda \text{ at bottom-left} \\ = \text{yellow diamond with diagonal} + \text{yellow diamond with diagonal} + x \text{ yellow diamond with arc on right} + x^{-1} \text{ yellow diamond with arc on left} \end{array} \quad (3.7b)$$

Acting vertically, the first operator acts as the identity and the second, acting at position j , acts as the Temperley–Lieb generator e_j .

More conventionally, the bulk face weights of the six vertex model are

$$\begin{aligned} W\left(\begin{array}{c|c} 0 & 0 \\ \hline 0 & 0 \end{array} \middle| z, g\right) &= 0 \begin{array}{c} 0 \\ \square \\ 0 \end{array} = 0 \begin{array}{c} 0 \\ \square \\ 0 \end{array} = s_1(-u) \\ W\left(\begin{array}{c|c} 1 & 0 \\ \hline 0 & 1 \end{array} \middle| z, g\right) &= 0 \begin{array}{c} 1 \\ \square \\ 1 \end{array} = 0 \begin{array}{c} 1 \\ \square \\ 1 \end{array} = s_0(u) \\ W\left(\begin{array}{c|c} 0 & 1 \\ \hline 1 & 0 \end{array} \middle| z, g\right) &= 0 \begin{array}{c} 0 \\ \square \\ 1 \end{array} = 0 \begin{array}{c} 1 \\ \square \\ 0 \end{array} = g^{-1} \\ W\left(\begin{array}{c|c} 1 & 0 \\ \hline 1 & 0 \end{array} \middle| z, g\right) &= 1 \begin{array}{c} 1 \\ \square \\ 0 \end{array} = 1 \begin{array}{c} 0 \\ \square \\ 1 \end{array} = g \\ W\left(\begin{array}{c|c} 0 & 1 \\ \hline 1 & 0 \end{array} \middle| z, g\right) &= 1 \begin{array}{c} 0 \\ \square \\ 0 \end{array} = 1 \begin{array}{c} 0 \\ \square \\ 0 \end{array} = s_0(u) \\ W\left(\begin{array}{c|c} 1 & 1 \\ \hline 1 & 1 \end{array} \middle| z, g\right) &= 1 \begin{array}{c} 1 \\ \square \\ 1 \end{array} = 1 \begin{array}{c} 1 \\ \square \\ 1 \end{array} = s_1(-u) \end{aligned} \quad (3.8)$$

The set of six allowed (blue) faces is not invariant under rotations through 90° . There is therefore no crossing symmetry. Instead, we distinguish the set of six rotated faces (pink) by the position of the corner marked by the (red) arc. In the blue faces, the particles move up and to the right and, in the pink faces, they move up and to the left. A face weight is unchanged under a rotation if the face configuration and the marked corner are rotated together. Again, the colour of the faces is just for easy visual identification.

The six vertex face weights can be organized into an \check{R} -matrix. Explicitly, choosing the particular basis $\{(0, 0), (0, 1), (1, 0), (1, 1)\}$ gives

$$W \left(\begin{array}{c|c} a & d \\ b & c \end{array} \middle| z, g \right) = X(u, g)_{ab}{}^{dc}, \quad X(u, g) = \begin{pmatrix} s_1(-u) & 0 & 0 & 0 \\ 0 & g^{-1} & s_0(u) & 0 \\ 0 & s_0(u) & g & 0 \\ 0 & 0 & 0 & s_1(-u) \end{pmatrix} \quad (3.9a)$$

$$W \left(\begin{array}{c|c} a & d \\ b & c \end{array} \middle| z, g \right) = \tilde{X}(u, g)_{da}{}^{cb}, \quad \tilde{X}(u, g) = \begin{pmatrix} s_1(-u) & 0 & 0 & g^{-1} \\ 0 & 0 & s_0(u) & 0 \\ 0 & s_0(u) & 0 & 0 \\ g & 0 & 0 & s_1(-u) \end{pmatrix} \quad (3.9b)$$

Let us define

$$X_j(u, g) = I \otimes I \otimes \dots \otimes I \otimes X(u, g) \otimes I \dots \otimes I \otimes I \quad (3.10)$$

acting on $(\mathbb{C}^2)^{\otimes N}$ where $X(u, g)$ acts in the slots j and $j + 1$ and similarly for $\tilde{X}(u, g)$. Setting

$$X_j(u) = X_j(u, z) = s_1(-u) I + s_0(u) e_j \quad (3.11)$$

the generators of the linear Temperley–Lieb algebra are then

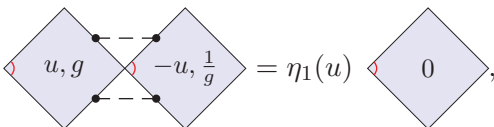
$$X_j(0) = I, \quad X_j(\lambda) = e_j, \quad j = 1, 2, \dots, N - 1 \quad (3.12)$$

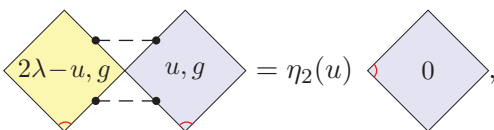
satisfying

$$e_j^2 = \beta e_j, \quad e_j e_{j \pm 1} e_j = e_j, \quad j = 1, 2, \dots, N - 1, \quad \beta = x + x^{-1}. \quad (3.13)$$

This corresponds to the linear vertical action of the planar algebra.

3.1.2. Inversion relations. The elementary face weights satisfy two distinct inversion relations. In the planar algebra, they are

Inv1 :  $\eta_1(u) = s_1(u) s_1(-u) \quad (3.14a)$

Inv2 :  $\eta_2(u) = s_0(u) s_2(-u) \quad (3.14b)$

In the linear algebra acting from left to right, these become

$$X_j(u, g) X_j(-u, 1/g) = s_1(u) s_1(-u) I \quad (3.15a)$$

$$\tilde{X}_j(2\lambda - u, g) \tilde{X}_j(u, g) = s_0(u) s_2(-u) I. \quad (3.15b)$$

Up to the scalar on the right side, the face $\tilde{X}_j(2\lambda - u, g)$ (shown in yellow) is the inverse of the face $\tilde{X}_j(u, g)$. We also observe the commutation relations

$$[X_j(u), X_j(v)] = 0, \quad [\tilde{X}_j(u, g), \tilde{X}_j(v, g)] = 0. \tag{3.16}$$

3.1.3. *Yang–Baxter equations.* The fundamental Yang–Baxter equation (YBE) [20] in the planar and linear algebra is

$$\tag{3.17a}$$

$$X_j(u)X_{j+1}(u+v)X_j(v) = X_{j+1}(v)X_j(u+v)X_{j+1}(u). \tag{3.17b}$$

Distorting the faces into rhombi leads to the alternative representation of the YBE as the following diagrammatic equality holding for all values of the indices $a, b, c, d, e, f = 0, 1$, of the two partition functions

$$\tag{3.18}$$

To establish commuting transfer matrices with Kac boundary conditions, we need three independent YBEs. In the planar algebra, these are

YBE1 :

$$\tag{3.19}$$

YBE2 :

$$\tag{3.20}$$

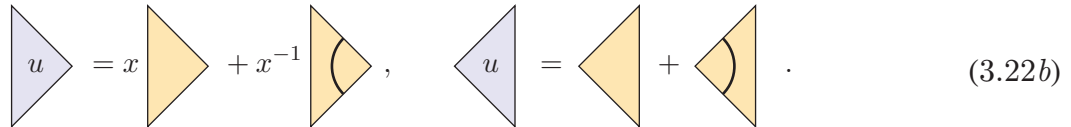
YBE3 :

$$\tag{3.21}$$

Here ξ is an arbitrary boundary field.

3.1.4. *Boundary Yang–Baxter equations.* In the presence of a boundary, there are additional local relations in the form of boundary Yang–Baxter or reflection equations [42, 43, 45]. The nonzero left and right boundary triangle weights and the corresponding planar operators are independent of u and given by

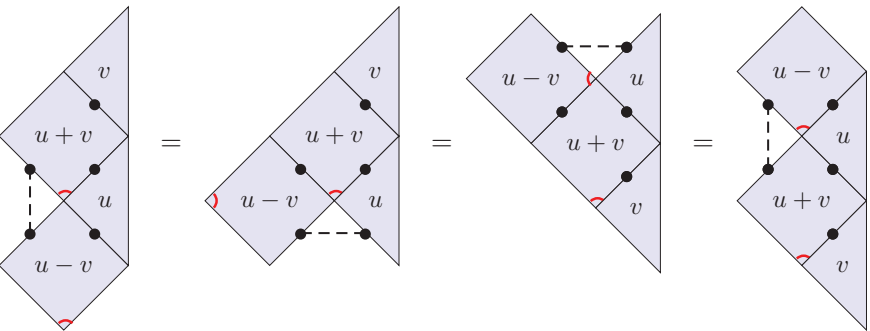
$$K^L\left(\begin{smallmatrix} b \\ a \end{smallmatrix}\right) = x^{1-2a}\delta(a, b), \quad K^R\left(\begin{smallmatrix} b \\ a \end{smallmatrix}\right) = \delta(a, b) \tag{3.22a}$$



$$\triangleleft_u = x \triangleleft_u + x^{-1} \triangleleft_u, \quad \triangleright_u = \triangleleft_u + \triangleright_u. \tag{3.22b}$$

The general right boundary Yang–Baxter equation (RBYBE) is

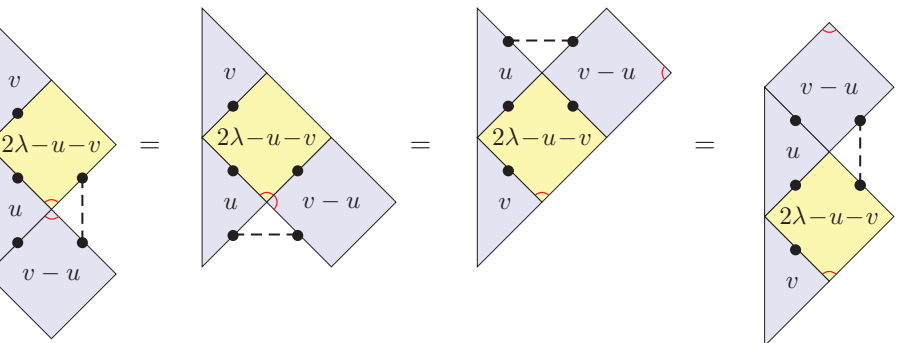
$$X_j(u - v)K_{j+1}^R(u)X_j(u + v)K_{j+1}^R(v) = K_{j+1}^R(v)X_j(u + v)K_{j+1}^R(u)X_j(u - v) \tag{3.23a}$$

RBYBE:  (3.23b)

where the relevant position is $j = N - 1$. After removing the right boundary triangles $K_{j+1}^R(u) = I$, this reduces to the commutation relation $[X_j(u - v), X_j(u + v)] = 0$.

With $z := e^{iu}$, $w := e^{iv}$, the general left boundary Yang–Baxter equation (LBYBE) is

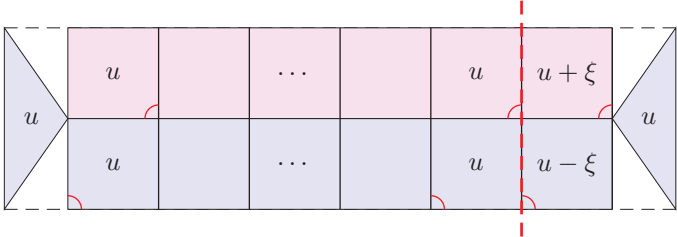
$$X_{j+1}(v - u, \frac{z}{w})K_j^L(u)\tilde{X}_{j+1}(2\lambda - u - v, zw)K_j^L(v) = K_j^L(v)\tilde{X}_{j+1}(2\lambda - u - v, zw)K_j^L(u)X_{j+1}(v - u, \frac{z}{w}) \tag{3.24a}$$

LBYBE:  (3.24b)

where the gauge factors have been omitted in the diagrams and the relevant position is $j = 0$. For the dimer model under consideration, the boundary triangles are independent of the spectral parameters.

3.2. Commuting double row transfer matrices

The general double row transfer matrices are defined diagrammatically by



$$D(u) = \begin{array}{c} \text{Diagrammatic representation of } D(u) \end{array} \quad (3.25)$$

where ξ is an arbitrary boundary field. There are a total of N columns in the bulk and $w = 0, 1$ columns in the boundary. We are primarily interested in the following two cases: (i) $w = 0$ in which case there is no boundary column and the system is homogeneous and (ii) $w = 1$ for which the boundary consists of the right-most column with $\xi = \frac{\lambda}{2}$. The specialization $\xi = \frac{\lambda}{2}$ has nice properties compared to other nonzero values of ξ . In particular, the inversion identity can be solved exactly for $\xi = \frac{\lambda}{2}$.

3.2.1. Sectors and quantum numbers. In the six vertex arrow (or spin) representation, the total magnetization

$$S_z = \sum_{j=1}^{\mathcal{N}} \sigma_j = -\mathcal{N}, -\mathcal{N} + 2, \dots, \mathcal{N} - 2, \mathcal{N}, \quad \mathcal{N} = N + w \quad (3.26)$$

is conserved under the action of the transfer matrix. By the \mathbb{Z}_2 up–down symmetry, the spectrum for the sectors $S_z = \pm m$ coincide for $m > 0$. More generally, the number of down spins is $d = \frac{1}{2}(\mathcal{N} - S_z)$. The number of up spins is thus $\mathcal{N} - d = \frac{1}{2}(\mathcal{N} + S_z)$ and the counting of states in the S_z sector is given by the binomial $\binom{\mathcal{N}}{d}$ with $S_z = \mathcal{N} \bmod 2$. In the particle representation, a particle configuration along a row of the double row transfer matrix takes the form

$$a = \{a_1, a_2, \dots, a_{\mathcal{N}-1}, a_{\mathcal{N}}\}, \quad a_j = 0, 1 \text{ for } j = 1, 2, \dots, \mathcal{N}. \quad (3.27)$$

The total number of particles $d = \sum_{j=1}^{\mathcal{N}} a_j$ coincides with the number of down arrows and is also conserved. The transfer matrix and vector space of states thus decompose as

$$D(u) = \bigoplus_{d=0}^{\mathcal{N}} D_d(u), \quad \dim \mathcal{V}^{(\mathcal{N})} = \sum_{d=0}^{\mathcal{N}} \dim \mathcal{V}_d^{(\mathcal{N})} = \sum_{d=0}^{\mathcal{N}} \binom{\mathcal{N}}{d} = 2^{\mathcal{N}} = \dim (\mathbb{C}^2)^{\otimes \mathcal{N}}. \quad (3.28)$$

For comparing the spectra sector-by-sector with critical dense polymers [33], it is useful to define

$$\ell = |\mathcal{N} - 2d| = |S_z| = \begin{cases} 0, 2, 4, \dots, \mathcal{N}, & \mathcal{N} \text{ even} \\ 1, 3, 5, \dots, \mathcal{N}, & \mathcal{N} \text{ odd} \end{cases}. \quad (3.29)$$

In the context of critical dense polymers, ℓ is the number of defects.

3.2.2. *Diagrammatic proof of commutation.* Setting $\eta_1 = \eta_1(u - v), \eta_2 = \eta_2(u + v)$ as in (3.14), the commutation of the double row transfer matrices is established diagrammatically

$$D(u)D(v) = \begin{array}{|c|c|c|c|c|c|} \hline & v & v & \dots & v & v + \xi \\ \hline v & & & & & \\ \hline & v & v & \dots & v & v - \xi \\ \hline & & & & & \\ \hline & u & u & \dots & u & u + \xi \\ \hline u & & & & & \\ \hline & u & u & \dots & u & u - \xi \\ \hline & & & & & \\ \hline \end{array} \quad (3.30a)$$

$$\stackrel{\text{Inv2}}{=} \frac{1}{\eta_2} \begin{array}{|c|c|c|c|c|c|} \hline & v & v & \dots & v & v + \xi \\ \hline v & & & & & \\ \hline & 2\lambda - u - v & u + v & & & \\ \hline & & & & & \\ \hline & v & v & \dots & v & v - \xi \\ \hline & & & & & \\ \hline & u & u & \dots & u & u + \xi \\ \hline u & & & & & \\ \hline & u & u & \dots & u & u - \xi \\ \hline & & & & & \\ \hline \end{array} \quad (3.30b)$$

$$\stackrel{\text{YBE1}}{=} \frac{1}{\eta_2} \begin{array}{|c|c|c|c|c|c|} \hline & v & v & \dots & v & v + \xi \\ \hline v & & & & & \\ \hline & 2\lambda - u - v & & & & \\ \hline & & & & & \\ \hline & u & u & \dots & u & u + \xi \\ \hline & & & & & \\ \hline & v & v & \dots & v & v - \xi \\ \hline & & & & & \\ \hline & u & u & \dots & u & u - \xi \\ \hline & & & & & \\ \hline \end{array} \quad (3.30c)$$

$\underline{\underline{\text{Inv1}}} \frac{1}{\eta_1 \eta_2}$

(3.30d)

$\underline{\underline{\text{YBE2}}} \frac{1}{\eta_1 \eta_2}$

(3.30e)

$\underline{\underline{\text{BYBE}}} \frac{1}{\eta_1 \eta_2}$

(3.30f)

$\underline{\underline{\text{YBE3}}} \frac{1}{\eta_1 \eta_2}$

(3.30g)

J. Stat. Mech. (2020) 013107

$$\text{Inv1} \frac{1}{\eta_2} \quad \begin{array}{c} \text{Diagram (3.30h)} \end{array} \quad (3.30h)$$

$$\text{YBE1} \frac{1}{\eta_2} \quad \begin{array}{c} \text{Diagram (3.30i)} \end{array} \quad (3.30i)$$

$$\text{Inv2} \quad \begin{array}{c} \text{Diagram (3.30j)} \end{array} = D(v)D(u) \quad (3.30j)$$

4. Solution of dimers on a strip and finite-size spectra

In this section, we specialise to the six vertex model at the free-fermion point with $\lambda = \frac{\pi}{2}$ and $x = i$ corresponding to dimers.

4.1. Inversion identities on the strip

In appendix A, we show that the double row transfer matrices (3.25) satisfy the inversion identities

$$w = 0 : \quad \mathbf{D}(u)\mathbf{D}(u + \lambda) = -\tan^2 2u \left[\cos^{2N} u - \sin^{2N} u \right]^2 \mathbf{I} \tag{4.1}$$

$$w = 1 : \quad \mathbf{D}(u)\mathbf{D}(u + \lambda) = -\tan^2 2u \left[\sin(u + \xi) \sin(u - \xi) \cos^{2N} u - \cos(u + \xi) \cos(u - \xi) \sin^{2N} u \right]^2 \mathbf{I}. \tag{4.2}$$

The first inversion identity is obtained from the second by dividing both sides by $\cos^4 \xi$ and taking the braid limit $\xi \rightarrow i\infty$. It is useful to introduce the normalized transfer matrices

$$\mathbf{d}(u) = \begin{cases} \frac{\mathbf{D}(u)}{\sin 2u}, & w = 0 \\ \frac{\mathbf{D}(u)}{\sin^2(\xi+\lambda) \sin 2u}, & w = 1 \end{cases} \tag{4.3}$$

satisfying the initial condition and crossing symmetry

$$\mathbf{d}(0) = \mathbf{I}, \quad \mathbf{d}(\lambda - u) = \mathbf{d}(u). \tag{4.4}$$

Remarkably, the normalized double row transfer matrices (4.3) satisfy precisely the same inversion identities as critical dense polymers [31, 34]. Specifically, we find

$$w = 0 : \quad \mathbf{d}(u) = \frac{\mathbf{D}(u)}{\sin 2u}, \quad \mathbf{d}(u)\mathbf{d}(u + \lambda) = \left(\frac{\cos^{2N} u - \sin^{2N} u}{\cos^2 u - \sin^2 u} \right)^2 \mathbf{I} \tag{4.5a}$$

$$w = 1, \quad \xi = \frac{\lambda}{2} : \quad \mathbf{d}(u) = \frac{2\mathbf{D}(u)}{\sin 2u}, \quad \mathbf{d}(u)\mathbf{d}(u + \lambda) = (\cos^{2N} u + \sin^{2N} u)^2 \mathbf{I}. \tag{4.5b}$$

Using standard inversion identity techniques [20, 28, 29], the last two functional equations can be solved, for arbitrary finite sizes N , for the eigenvalues $d(u)$ of $\mathbf{d}(u)$. The calculation of the eigenvalues by solving the functional equations (4.5a) and (4.5b) follows exactly the same path as in [34]. So let us just summarize the salient facts. The eigenvalues $d(u)$ are Laurent polynomials in $z = e^{iu}$. Consequently, they are determined by their complex zeros in the analyticity strip $-\frac{\pi}{4} \leq \text{Re } u \leq \frac{3\pi}{4}$. Following [34], these zeros occur as 1-strings in the center of the analyticity strip or as ‘2-strings’ with one zero on the boundary $\text{Re } u = -\frac{\pi}{4}$ of the analyticity strip and its periodic image on the other boundary $\text{Re } u = \frac{3\pi}{4}$. The ordinates of the 1- and 2-strings are quantized and given by

$$y_j = -\frac{i}{2} \ln \tan \frac{E_j \pi}{2N}, \quad E_j = \begin{cases} j, & N + w \text{ even} \\ j - \frac{1}{2}, & N + w \text{ odd} \end{cases} \quad j \in \mathbb{Z}. \tag{4.6}$$

At each allowed ordinate, there is either two 1-strings, two 2-strings or one 1-string and one 2-string. The fact that double zeros occur has its origins in the relation between critical dense polymers and symplectic fermions [46]. Due to complex conjugation symmetry, the pattern of zeros in the upper and lower half-planes is the same. We can therefore focus solely on the lower half-plane. A typical pattern of zeros is shown in figure 6.

A pattern of zeros is completely determined by specifying the location of the 1-strings. A 1-string at position j is a local elementary excitation with associated conformal energy E_j . In the ground state, with energy E_0 , there are no 1-strings. Counting

the doubled 1-strings as two separate 1-strings, the conformal excitation energy above the ground state is given by

$$E = E_0 + \sum_j E_j, \quad j = \text{position of 1-strings.} \tag{4.7}$$

The lowest state energy is $E_0 = -\frac{c}{24} + \Delta_s$ where c is the central charge and Δ_s is the conformal weight associated with the particular sector labelled by

$$s = |S_z| + 1, \quad \mathcal{N} + s \text{ odd.} \tag{4.8}$$

The lowest states in each sector exactly coincide with those of critical dense polymers for arbitrary finite sizes. The zero patterns for these lowest states are encoded as double column diagrams in figure 7. On the strip, the only difference between dimers and critical dense polymers with $(r, s) = (1, 1)$ boundary conditions resides in the degeneracy of energy levels and the counting of states. The finite-size corrections based on Euler–Maclaurin calculations therefore also coincide, yielding $c_{\text{eff}} = 1$. As justified in section 5, we conclude that the central charge is $c = -2$ and the conformal weights are $\Delta_s = ((2 - s)^2 - 1)/8$ with $s = 1, 2, 3, \dots$

It follows that the finitized characters take the form

$$\chi_s^{(N)}(q) = q^{-c/24 + \Delta_s} \sum_E q^E, \quad E = \text{eigenvalue excitation energy.} \tag{4.9}$$

This is a truncated set of conformal eigenenergies of the infinite system. The finitized characters are the spectrum generating functions for the finite set of conformal energies. The parameter q is the modular nome and arises through the finite-size calculation as

$$q = \exp\left(-2\pi \frac{N'}{N} \sin 2u\right) \tag{4.10}$$

where N'/N is the fixed lattice aspect ratio. The remaining problem is thus to classify the allowed patterns of zeros and their degeneracies. This is a combinatorial problem and, since not all patterns of zeros occur, it entails certain selection rules. We determine the classification of zero patterns empirically based on examining the patterns of zeros for modest sizes N . For critical dense polymers on the strip, the empirical selection rules obtained were ultimately shown to be correct [47].

4.2. Combinatorial analysis of patterns of zeros

Combinatorially, the key building blocks are q -Narayana numbers (or equivalently skew q -binomials) enumerated by double-column diagrams with dominance.

The information in a zero pattern is simply encoded in a double-column diagram. A double-column configuration $S = (L, R)$ is called *admissible* if $L \preceq R$ with respect to the partial ordering

$$L \preceq R \quad \text{if} \quad L_j \leq R_j, \quad j = 1, 2, \dots, m \tag{4.11}$$

which presupposes that

$$0 \leq m \leq n \leq M. \tag{4.12}$$

Admissibility is characterized diagrammatically as in the following example

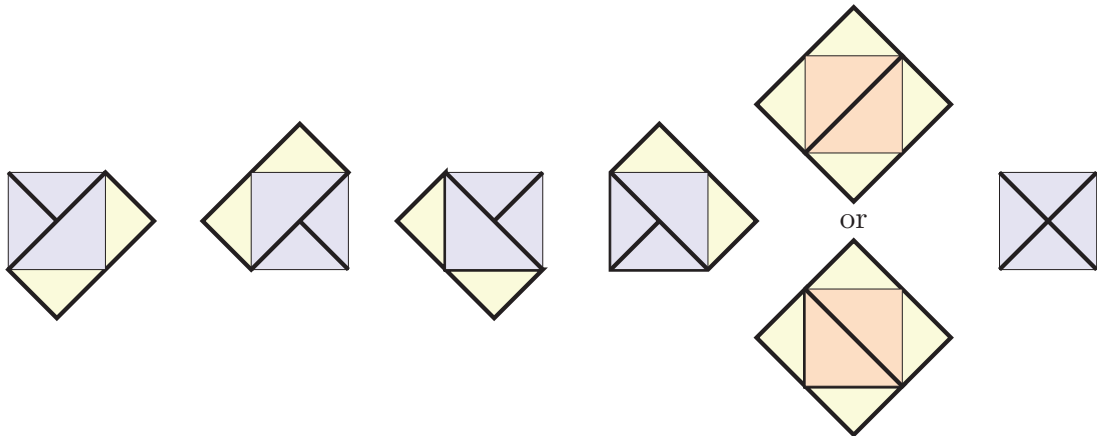
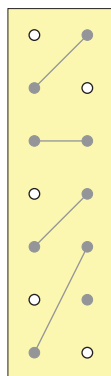


Figure 4. Face configurations showing (in light yellow) the one or two dimers associated with each face. No dimers are associated with the last face.



(4.13)

One draws line segments between the occupied sites of greatest height in the two columns, then between the occupied sites of second-to-greatest height and so on. The double-column configuration is now admissible if $m \leq n$ and it does *not* involve line segments with a *strictly negative slope*. Thus, in an admissible double-column configuration, there are either no line segments ($m = 0$) or each line segment appears with a non-negative slope. Such admissible diagrams are said to satisfy dominance. At each position or height j , there is zero, one or two occupied sites corresponding to zero, one or two 1-strings in the lower half-plane.

Combinatorially, the (generalized) q -Narayana numbers $\left\langle \begin{matrix} M \\ m, n \end{matrix} \right\rangle_q$ are defined as the sum of the monomials associated to all admissible double-column configurations of height M with exactly m and n occupied sites in the left and right columns, respectively

$$\left\langle \begin{matrix} M \\ m, n \end{matrix} \right\rangle_q = \sum_{S: |L|=m, |R|=n} q^{E(S)}. \tag{4.14}$$

These are the basic building blocks to describe the allowed patterns of zeros in each sector. Physically, these are the generating functions for the spectrum encoded in a double column diagram with conformal energies $E_j = j$. The monomials $q^{E(S)}$ need to be scaled

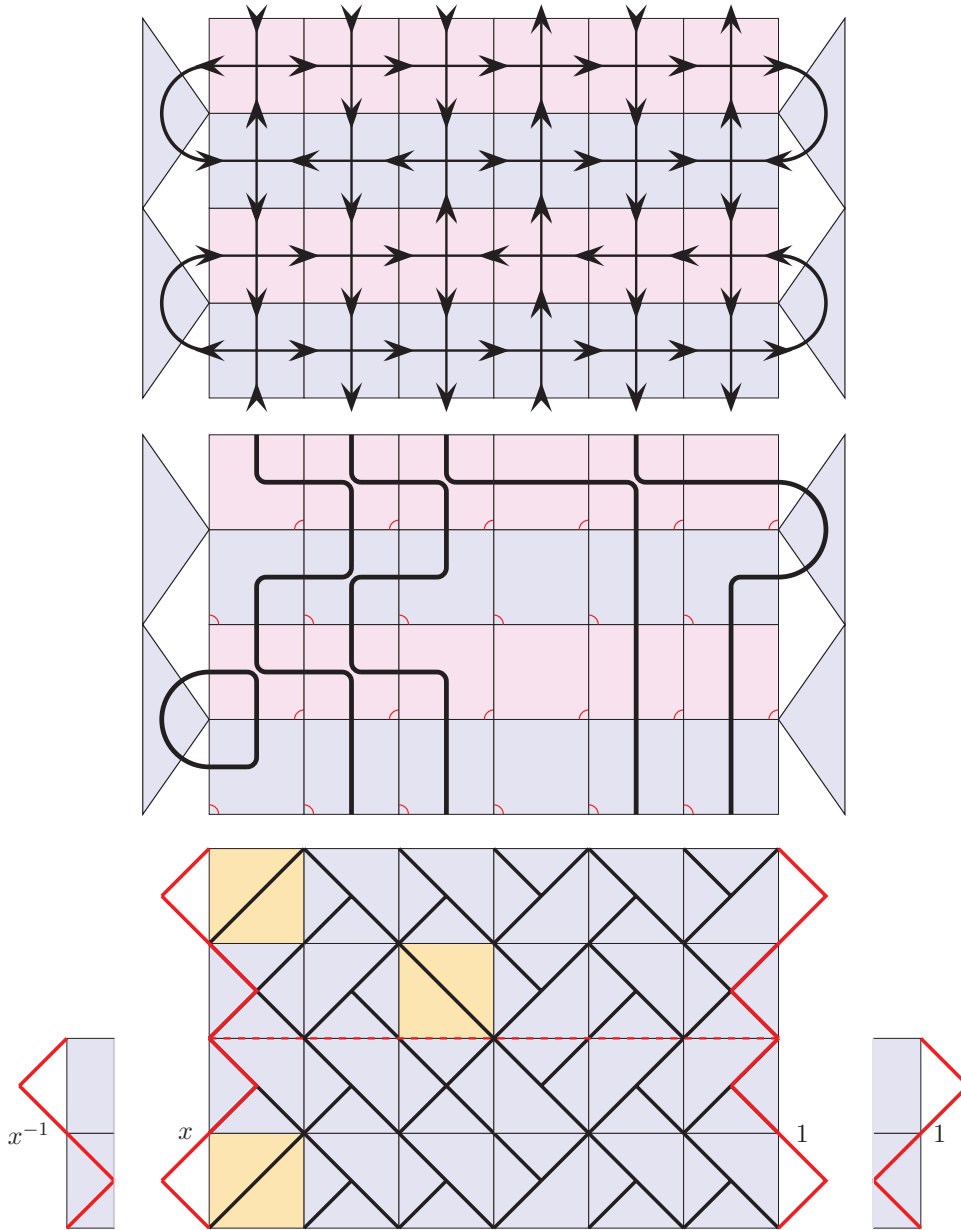


Figure 5. Typical dimer configuration on a 6×4 strip with vacuum boundary conditions in the vertex, particle and dimer representations. For the vertex representation, the boundary arrows can be in either one of the two possible directions (corresponding to a particle or vacancy in the particle representation). Particles move up and right on odd rows and up and left on even rows. The number of particles/down arrows inside the strip is conserved from double row to double row but not necessarily from single row to single row. For dimers, there are two different zigzag edges allowed independently on the left and right edges of each double row. The left boundary zigzags have weights x, x^{-1} as shown. The right boundary zigzags have weight 1.

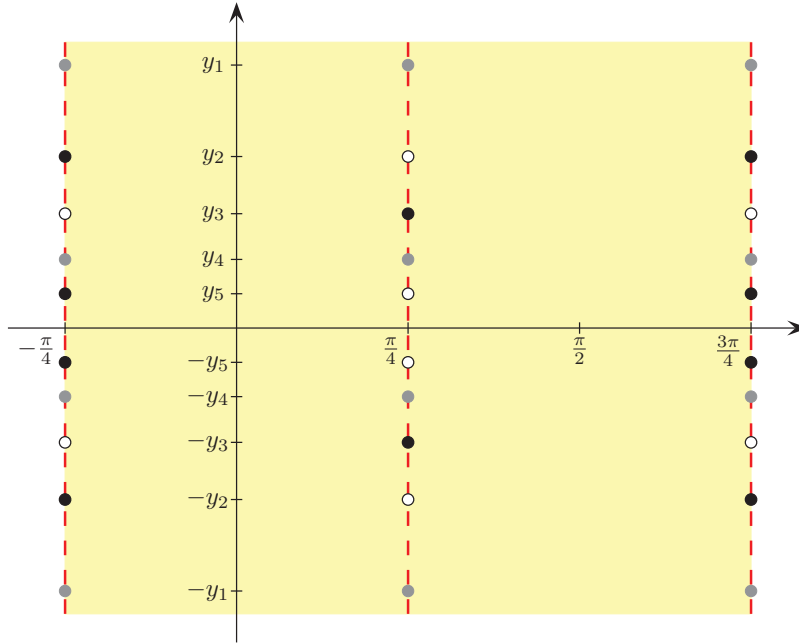


Figure 6. A typical pattern of zeros in the complex u -plane associated to a transfer matrix eigenvalue. Single zeros are shown by grey disks, double zeros are shown by black disks and the absence of zeros is shown by white disks. The upper and lower half-planes are related under the \mathbb{Z}_2 complex conjugation symmetry.

by the factor $q^{-\frac{1}{2}(m+n)}$ in sectors with $E_j = j - \frac{1}{2}$. The q -Narayana numbers admit the closed-form expressions

$$\left\langle \begin{matrix} M \\ m, n \end{matrix} \right\rangle_q = q^{\frac{1}{2}m(m+1) + \frac{1}{2}n(n+1)} \left\{ \begin{matrix} M \\ m, n \end{matrix} \right\}_q \tag{4.15}$$

$$= q^{\frac{1}{2}m(m+1) + \frac{1}{2}n(n+1)} \left(\left[\begin{matrix} M \\ m \end{matrix} \right]_q \left[\begin{matrix} M \\ n \end{matrix} \right]_q - q^{n-m+1} \left[\begin{matrix} M \\ m-1 \end{matrix} \right]_q \left[\begin{matrix} M \\ n+1 \end{matrix} \right]_q \right) \tag{4.16}$$

where $\left[\begin{matrix} M \\ m \end{matrix} \right]_q$ is a q -binomial (Gaussian polynomial) and $\left\{ \begin{matrix} M \\ m, n \end{matrix} \right\}_q$ are skew q -binomials, as in appendix B. The (generalized) q -Narayana numbers coincide with q -Narayana numbers [48, 49] when $m = n$.

4.3. Empirical selection rules

In this section we consider the empirical classification of patterns of zeros for the cases $w = 0, 1$. Empirically, using Mathematica [38] to examine the spectra out to $\mathcal{N} = N + w = 8$, we find that the finitized characters are classified in terms of patterns of zeros, double column diagrams and q -Narayana numbers by

$$\chi_s^{(N)}(q) = \begin{cases} q^{-c/24 + \Delta_1} \sum_{m,n=0}^{\lfloor \frac{\mathcal{N}-1}{2} \rfloor} A_{m,n}^{(s)} \left\langle \begin{matrix} \lfloor \frac{\mathcal{N}-1}{2} \rfloor \\ m, n \end{matrix} \right\rangle_q, & \Delta_1 = 0, s \text{ odd} \\ q^{-c/24 + \Delta_2} \sum_{m,n=0}^{\lfloor \frac{\mathcal{N}-1}{2} \rfloor} B_{m,n}^{(s)} q^{-\frac{1}{2}(m+n)} \left\langle \begin{matrix} \lfloor \frac{\mathcal{N}-1}{2} \rfloor \\ m, n \end{matrix} \right\rangle_q, & \Delta_2 = -\frac{1}{8}, s \text{ even} \end{cases} \tag{4.17}$$

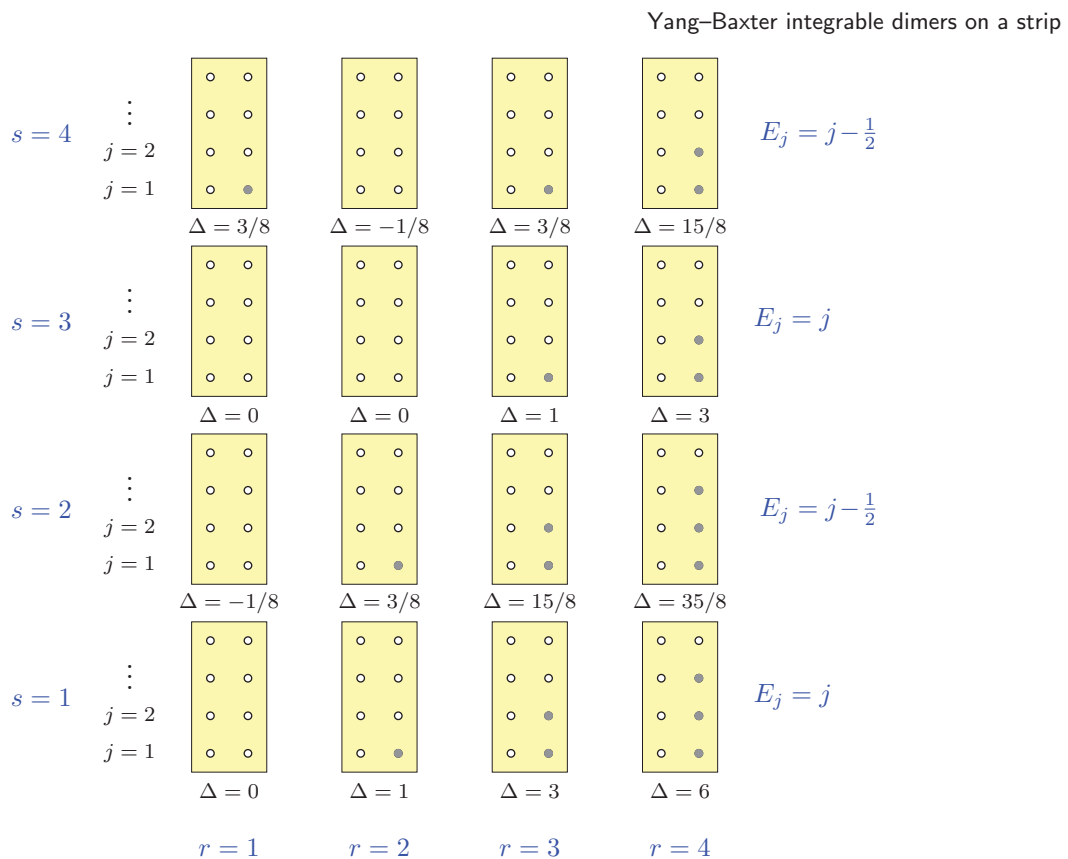


Figure 7. Lowest or groundstate double-column configurations arranged by sectors in a Kac table for $r, s = 1, 2, 3, 4$ for critical dense polymers. The continuation of the pattern for larger values of r and s is clear. Only the first column with $r = 1$ relates to dimers. The solid grey dots represent single 1-strings in the center of the analyticity strip. There are no double zeros in the center of the analyticity strip for these groundstates. The vacuum sector with $\Delta = 0$ lies at $(r, s) = (1, 1)$.

The $\lfloor \frac{\mathcal{N}+1}{2} \rfloor \times \lfloor \frac{\mathcal{N}+1}{2} \rfloor$ matrices $A^{(s)}$ and $B^{(s)}$ are special Toeplitz matrices with a simple structure as indicated in the following examples

$$\mathcal{N} = 8: A^{(1)} = \begin{pmatrix} 2 & 2 & 2 & 2 \\ 0 & 2 & 2 & 2 \\ 0 & 0 & 2 & 2 \\ 0 & 0 & 0 & 2 \end{pmatrix}, A^{(3)} = \begin{pmatrix} 1 & 2 & 2 & 2 \\ 0 & 1 & 2 & 2 \\ 0 & 0 & 1 & 2 \\ 0 & 0 & 0 & 1 \end{pmatrix}, A^{(5)} = \begin{pmatrix} 0 & 1 & 2 & 2 \\ 0 & 0 & 1 & 2 \\ 0 & 0 & 0 & 1 \\ 0 & 0 & 0 & 0 \end{pmatrix}, \dots,$$

$$A^{(9)} = \begin{pmatrix} 0 & 0 & 0 & 1 \\ 0 & 0 & 0 & 0 \\ 0 & 0 & 0 & 0 \\ 0 & 0 & 0 & 0 \end{pmatrix} \tag{4.18}$$

$$\mathcal{N} = 7: \quad B^{(2)} = \begin{pmatrix} 1 & 1 & 1 & 1 \\ 0 & 1 & 1 & 1 \\ 0 & 0 & 1 & 1 \\ 0 & 0 & 0 & 1 \end{pmatrix}, \quad B^{(4)} = \begin{pmatrix} 0 & 1 & 1 & 1 \\ 0 & 0 & 1 & 1 \\ 0 & 0 & 0 & 1 \\ 0 & 0 & 0 & 0 \end{pmatrix}, \quad B^{(6)} = \begin{pmatrix} 0 & 0 & 1 & 1 \\ 0 & 0 & 0 & 1 \\ 0 & 0 & 0 & 0 \\ 0 & 0 & 0 & 0 \end{pmatrix},$$

$$B^{(8)} = \begin{pmatrix} 0 & 0 & 0 & 1 \\ 0 & 0 & 0 & 0 \\ 0 & 0 & 0 & 0 \\ 0 & 0 & 0 & 0 \end{pmatrix}.$$

(4.19)

Following [33], for $r \geq 1$, we define the following (generalized) q -analogs of Catalan numbers

$$C_{M,r}(q) = \sum_{m=0}^{M-r+1} \left\langle \begin{matrix} M \\ m, m+r-1 \end{matrix} \right\rangle_q = q^{\frac{r(r-1)}{2}} \frac{(1-q^r)}{(1-q^{M+1})} \left[\begin{matrix} 2M+2 \\ M+1-r \end{matrix} \right]_q \quad s \text{ odd}$$

$$C'_{M,r}(q) = q^{-\frac{r-1}{2}} \sum_{m=0}^{M-r+1} q^{-m} \left\langle \begin{matrix} M \\ m, m+r-1 \end{matrix} \right\rangle_q = q^{\frac{(r-1)^2}{2}} \frac{(1-q^{2r})}{(1-q^{M+r+1})} \left[\begin{matrix} 2M+1 \\ M+1-r \end{matrix} \right]_q \quad s \text{ even}$$

(4.20)

These q -Catalan polynomials are simply related to finitized irreducible characters [34]

$$\text{ch}_{r,1}^{(M)}(q) = q^{-\frac{c}{24}} C_{M,r}(q), \quad \text{ch}_{r,2}^{(M)}(q) = q^{-\frac{c}{24} - \frac{1}{8}} C'_{M,r}(q).$$

(4.21)

Using the result

$$\lim_{M \rightarrow \infty} \left[\begin{matrix} M \\ m \end{matrix} \right]_q = \frac{1}{(q)_m}, \quad (q)_m = \prod_{k=1}^m (1 - q^k)$$

(4.22)

it follows from (4.20) that, in the thermodynamic limit, the irreducible characters are

$$\text{ch}_{r,1}(q) = \lim_{M \rightarrow \infty} \text{ch}_{r,1}^{(M)}(q) = q^{-\frac{c}{24} + \frac{r(r-1)}{2}} \frac{1 - q^r}{(q)_\infty}$$

(4.23)

$$\text{ch}_{r,2}(q) = \lim_{M \rightarrow \infty} \text{ch}_{r,2}^{(M)}(q) = q^{-\frac{c}{24} - \frac{1}{8} + \frac{(r-1)^2}{2}} \frac{1 - q^{2r}}{(q)_\infty}.$$

(4.24)

Summing over diagonals in (4.17) with $n - m = r - 1 \geq 0$ gives the decomposition into finitized irreducible characters

$$\chi_s^{(N)}(q) = \begin{cases} \sum_{r=1}^{\lfloor \frac{N+1}{2} \rfloor} A_{1,r}^{(s)} \text{ch}_{r,1}^{(M)}(q), & s \text{ odd} \\ \sum_{r=1}^{\lfloor \frac{N+1}{2} \rfloor} B_{1,r}^{(s)} \text{ch}_{r,2}^{(M)}(q), & s \text{ even} \end{cases} \quad M = \lfloor \frac{\mathcal{N} - 1}{2} \rfloor.$$

(4.25)

For $w = 0, 1$ and s odd or even, the finitized characters can be written in terms of q -binomials

$$\chi_s^{(N)}(q) = q^{-c/24 + \Delta_s} \frac{1 + q^{(s-1)/2}}{1 + q^{N/2}} \left[\begin{matrix} \mathcal{N} \\ \frac{1}{2}(\mathcal{N} + s - 1) \end{matrix} \right]_q, \quad \mathcal{N} = N + w$$

(4.26)

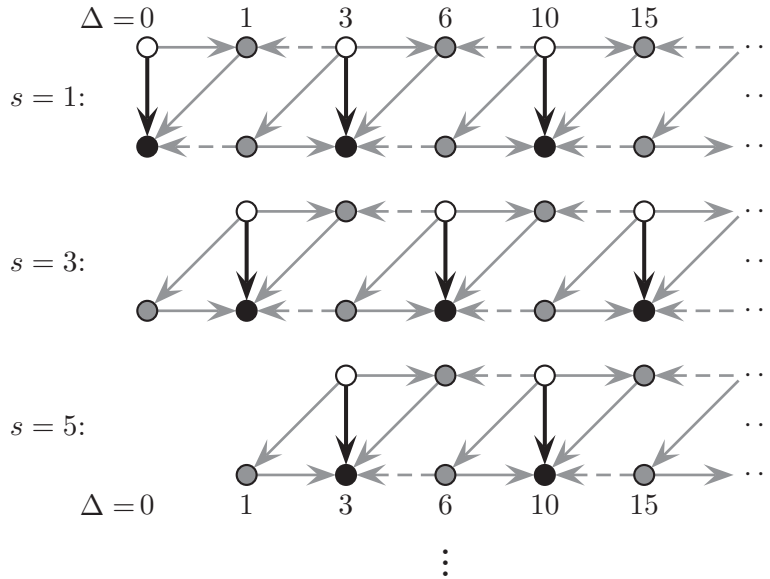


Figure 8. Loewy diagrams of the Virasoro modules \mathcal{D}_s for $s = 1, 3, 5, \dots$. The nodes represent irreducible sub-quotients, or equivalently, sub-singular vectors generating these sub-quotients. The black arrows indicate the off-diagonal action of L_0 in the rank 2 Jordan blocks. The gray arrows indicate the conjectured action by the Virasoro algebra linking the irreducible sub-quotients.

where

$$\Delta_s = \frac{(2 - s)^2 - 1}{8}. \tag{4.27}$$

Setting $q = 1$ gives the correct counting of states $\chi_s^{(N)}(1) = \binom{\mathcal{N}}{\frac{1}{2}(\mathcal{N}+s-1)}$. Observing that $|q| < 1$ and using the result (4.22), it follows that, in the thermodynamic limit,

$$\chi_s(q) = \lim_{N \rightarrow \infty} \chi_s^{(N)}(q) = \frac{q^{-c/24 + \Delta_s}}{(q)_\infty} (1 + q^{(s-1)/2}) = \frac{q^{-c/24}}{(q)_\infty} (q^{\Delta_s} + q^{\Delta_{s+2}}). \tag{4.28}$$

Notice that, for $s = 1$, all states are doubly degenerate and that, for s even, $q^{(s-1)/2}$ is a half-integer power of q .

5. Jordan decompositions and irreducible modules

5.1. Isotropic double row transfer matrices

It is easy to verify that, at the isotropic point $u = \frac{\lambda}{2}$, the double row transfer matrix $\mathbf{D}(u)$ is not Hermitian. Nevertheless, it has real eigenvalues. For \mathcal{N} odd, we find no Jordan blocks. But, for \mathcal{N} even, we find the Jordan decomposition produces nontrivial Jordan blocks of rank 2. Explicitly, for $w = 0$ and $\mathcal{N} = N$ even,

$$\mathcal{N} = 2, S_z = 0 : \quad \begin{pmatrix} 1 & 1 \\ 0 & 1 \end{pmatrix} \tag{5.1}$$

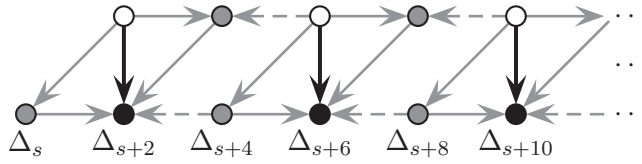


Figure 9. Loewy diagram for s odd with $s > 1$.

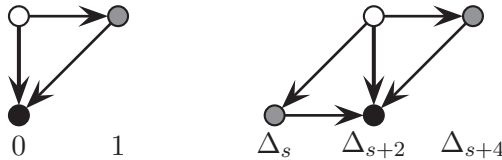


Figure 10. Staggered modules for $c = -2$, corresponding respectively to $s = 1$ and $s = 3, 5, \dots$

$$\mathcal{N} = 4, S_z = 0 : \quad \frac{1}{2} \oplus \begin{pmatrix} \frac{3}{2} - \sqrt{2} & 1 \\ 0 & \frac{3}{2} - \sqrt{2} \end{pmatrix} \oplus \begin{pmatrix} \frac{3}{2} + \sqrt{2} & 1 \\ 0 & \frac{3}{2} + \sqrt{2} \end{pmatrix} \oplus \frac{1}{2} \tag{5.2}$$

with similar results for $w = 1$, N odd and $\xi = \frac{\lambda}{2}$.

5.2. Quantum Hamiltonians

The quantum Hamiltonians are given by the logarithmic derivative

$$\mathcal{H}_w = -\frac{1}{2} \frac{d}{du} \log \mathbf{D}(u) \Big|_{u=0}, \quad w = 0, 1. \tag{5.3}$$

As pointed out in [19], the Hamiltonian of dimers on the strip with $w = 0$ precisely coincides with the $U_q(\mathfrak{sl}(2))$ -invariant XX Hamiltonian of the free-fermion six vertex model

$$\mathcal{H}_{w=0} = -\sum_{j=1}^{N-1} e_j = -\frac{1}{2} \sum_{j=1}^{N-1} (\sigma_j^x \sigma_{j+1}^x + \sigma_j^y \sigma_{j+1}^y) - \frac{1}{2} i (\sigma_1^z - \sigma_N^z) \tag{5.4}$$

$$= -\sum_{j=1}^{N-1} (f_j^\dagger f_{j+1} + f_{j+1}^\dagger f_j) - i (f_1^\dagger f_1 - f_N^\dagger f_N) \tag{5.5}$$

where $\sigma_j^{x,y,z}$ are the usual Pauli matrices and $f_j = \frac{1}{2}(\sigma_j^x - i\sigma_j^y)$, $f_j^\dagger = \frac{1}{2}(\sigma_j^x + i\sigma_j^y)$. This Hamiltonian is manifestly not Hermitian. Nevertheless, the eigenvalues of the Hamiltonian are real [50]. For $\mathcal{N} = N$ odd, we find no non-trivial Jordan blocks but, for \mathcal{N} even, we find rank 2 Jordan blocks. Separating into $S_z = 0, \pm 2, \pm 4, \dots$ sectors and identifying the equivalent $\pm S_z$ sectors, the Jordan canonical forms for $\mathcal{N} = 2$ and $\mathcal{N} = 4$ are respectively

$$\mathcal{N} = 2 : \quad \left[\begin{pmatrix} 0 & 1 \\ 0 & 0 \end{pmatrix} \right] \oplus 2[0] \tag{5.6}$$

J. Stat. Mech. (2020) 013107

$$\mathcal{N} = 4 : \quad \left[\begin{pmatrix} \sqrt{2} & 1 \\ 0 & \sqrt{2} \end{pmatrix} \oplus 0 \oplus 0 \oplus \begin{pmatrix} -\sqrt{2} & 1 \\ 0 & -\sqrt{2} \end{pmatrix} \right] \oplus 2[\sqrt{2} \oplus \begin{pmatrix} 0 & 1 \\ 0 & 0 \end{pmatrix} \oplus (-\sqrt{2})] \oplus 2[0]. \quad (5.7)$$

Such Jordan blocks for the quantum group invariant XX Hamiltonian were observed in [51]. More generally, we find empirically that there are $\binom{N-2}{d-1}$ rank 2 Jordan blocks in sectors with d down arrows where $1 \leq d \leq N - 1$, in accordance with [47]. By comparison, the transfer matrices and Hamiltonians of the (r, s) sectors of critical dense polymers are diagonalizable [31] and do not exhibit Jordan blocks.

The Hamiltonian of dimers on the strip with $w = 1$ agrees with the $\rho = 2$ Hamiltonian of critical dense polymers [34]

$$\mathcal{H}_{w=1} = - \sum_{j=1}^{N-1} e_j + \frac{1}{s_0(\xi)s_2(\xi)} e_N. \quad (5.8)$$

This can be written in terms of fermion operators using (2.13c). Specializing to $\xi = \frac{\lambda}{2} = \frac{\pi}{4}$, we find no Jordan blocks for $\mathcal{N} = N + 1$ odd but rank 2 Jordan blocks for \mathcal{N} even

$$\mathcal{N} = 2 : \quad \left[\begin{pmatrix} 0 & 1 \\ 0 & 0 \end{pmatrix} \right] \oplus 2[0] \quad (5.9)$$

$$\mathcal{N} = 4 : \quad \left[\begin{pmatrix} \sqrt{3} & 1 \\ 0 & \sqrt{3} \end{pmatrix} \oplus 0 \oplus 0 \oplus \begin{pmatrix} -\sqrt{3} & 1 \\ 0 & -\sqrt{3} \end{pmatrix} \right] \oplus 2[\sqrt{3} \oplus \begin{pmatrix} 0 & 1 \\ 0 & 0 \end{pmatrix} \oplus (-\sqrt{3})] \oplus 2[0]. \quad (5.10)$$

Although the eigenvalues are different, the patterns of the appearance of Jordan blocks is the same as for $w = 0$. This is easily seen for $\mathcal{N} = 2, 4$ by comparing (5.6) and (5.7) with (5.9) and (5.10).

5.3. Representation theory

In the continuum scaling limit, the $w = 0$ and $w = 1$ Hamiltonians give rise to the Virasoro dilatation operator L_0 . For s even (\mathcal{N} odd), we do not find any non-trivial Jordan blocks. For s odd (\mathcal{N} even), on the other hand, we *do* find non-trivial Jordan blocks, all of rank 2. Since the indications are that these Jordan blocks persist in the scaling limit, we see that the dimer model admits higher-rank representations of the Virasoro algebra. We thus conclude that, as a CFT, our dimer model is *logarithmic*.

Restricting to s odd and analysing the patterns of appearance of the Jordan blocks yields crucial insight into the structures of the ensuing Virasoro modules, here denoted by \mathcal{D}_s , $s = 1, 3, 5, \dots$. Although not uniquely determined, see comment below, the Loewy diagrams in figures 8 and 9 are compatible with this analysis and with the results for the finitized characters. Thus, in the Loewy diagram indicated for \mathcal{D}_s , the black dots represent singular vectors which generate the socle C^\bullet , i.e. the maximal completely reducible submodule of \mathcal{D}_s . The gray dots represent sub-singular vectors that are singular in the quotient \mathcal{D}_s/C^\bullet ; they generate the socle C^* of \mathcal{D}_s/C^\bullet . Finally, the white dots represent sub-singular vectors that are singular in $(\mathcal{D}_s/C^\bullet)/C^*$; they generate the head, i.e. the maximal completely reducible quotient of \mathcal{D}_s .

We note that our analysis so far is incapable of determining whether the left-pointing horizontal (dashed) arrows, in particular, are actually present in the diagrams

for \mathcal{D}_s in figures 8 and 9. As drawn, the diagrams describe *indecomposable* modules, whereas the diagrams obtained by removing the left-pointing horizontal arrows would describe *decomposable* modules. The latter option is supported by the analysis in [41]. However, independent of the presence of these arrows, the familiar $c = -2$ staggered modules [52] in figure 10 appear as *submodules* of our dimer modules \mathcal{D}_s . This resembles the way the Virasoro Kac modules [53] appear as submodules of the Feigin–Fuchs modules [54] arising in the dimer model [13]. It therefore seems natural to expect that modules similar to our dimer modules exist for other logarithmic minimal models as well.

Following the conjectured module structures (with or without the left-pointing horizontal arrows), the finitized characters $\chi_s^{(N)}(q)$ decompose into finitized characters of the irreducible sub-quotients of conformal weights $\Delta \in \{0, 1, 3, 6, 10, 15, \dots\}$. Parameterising these weights as

$$\Delta_{r,1} = \Delta_{2r+1} = \frac{(2r - 1)^2 - 1}{8}, \quad r = 1, 2, 3, \dots \tag{5.11}$$

the decompositions are given by (4.25), where the finitized irreducible characters are denoted by $\text{ch}_{r,1}^{(M)}(q)$ with $M = \lfloor \frac{N-1}{2} \rfloor$. We can refine these decompositions by indicating the appearances of the Jordan blocks. For simplicity, we do this for the full Virasoro characters. Similar expressions for the finitized characters follow readily. We thus write

$$\chi_s(q) = \begin{cases} \sum_{r \in 1+2\mathbb{Z}_{\geq 0}} \hat{2} \text{ch}_{r,1}(q) + \sum_{r \in 2+2\mathbb{Z}_{\geq 0}} 2 \text{ch}_{r,1}(q), & s = 1 \\ \text{ch}_{\frac{s-1}{2},1}(q) + \sum_{r \in \frac{s+1}{2}+2\mathbb{Z}_{\geq 0}} \hat{2} \text{ch}_{r,1}(q) + \sum_{r \in \frac{s+3}{2}+2\mathbb{Z}_{\geq 0}} 2 \text{ch}_{r,1}(q), & s = 3, 5, \dots \end{cases} \tag{5.12}$$

where a hat on a multiplicity, $\hat{2}$, indicates that Jordan blocks are formed between the matching vectors in the two copies of the corresponding irreducible sub-quotient.

6. Conclusion

Although the dimer model was first solved many years ago, there remain a number of unanswered questions concerning its CFT description. In a previous paper [19], the dimer model on a cylinder, with 45° rotated dimers, was solved exactly. Moreover, the modular invariant conformal partition function was obtained from finite-size corrections and shown to precisely agree with the modular invariant partition function of critical dense polymers.

In this paper, we have solved exactly the dimer model on a strip with $U_q(\mathfrak{sl}(2))$ invariant boundary conditions by viewing it as a free-fermion six vertex model and using Yang–Baxter techniques. The key to solving the lattice model is to show that the commuting double row transfer matrices satisfy special functional equations in the form of inversion identities. Due to the common underlying Temperley–Lieb algebra, these inversion identities coincide with those of critical dense polymers. This implies, essentially through the Temperley–Lieb equivalence, that the two models have the same eigenvalues, although the eigenvalue degeneracies and the counting of states differ. Indeed, the lowest eigenvalues in each sector (labelled by $(r, s) = (1, s)$) coincide leading to the same finite-size corrections. This leads us to conclude that, for the

$U_q(\mathfrak{sl}(2))$ invariant boundary conditions, the two models share the same central charge and a common infinite set of conformal weights

$$c = -2, \quad \Delta_s = \Delta_{1,s} = \frac{(2-s)^2 - 1}{8}, \quad s = 1, 2, 3, \dots \quad (6.1)$$

The common negative conformal weight

$$\Delta_2 = \Delta_{1,2} = -\frac{1}{8} \quad (6.2)$$

implies that both CFTs are nonunitary. However, despite these similarities, combinatorial analysis of the patterns of zeros of the transfer matrix eigenvalues of dimers on the strip leads to finitized and conformal characters (4.26) and (4.28) that are distinct from the Kac characters of critical dense polymers. So it appears that the dimer model, with these boundary conditions, lies in a different ‘universality class’ to that of critical dense polymers.

Moreover, we have shown that for dimers on the strip, with $U_q(\mathfrak{sl}(2))$ invariant boundary conditions, the Jordan canonical forms of the isotropic double row transfer matrices and quantum Hamiltonians exhibit nontrivial Jordan blocks. Assuming, as argued, that these Jordan blocks persist in the scaling limit, this implies that the dilatation operator L_0 admits higher-rank Virasoro representations. All this points to a CFT description of the dimer model that is not rational. Indeed, we argue that, with $U_q(\mathfrak{sl}(2))$ invariant boundary conditions, the model is described by a logarithmic CFT with central charge $c = -2$, minimal conformal weight $\Delta_{\min} = -\frac{1}{8}$ and effective central charge $c_{\text{eff}} = 1$.

Notwithstanding our conclusion, some additional comments are in order. First, we have chosen to apply boundary conditions (3.22) with $x = i$ compatible with $U_q(\mathfrak{sl}(2))$ invariance. Our boundary weights (3.22) are thus complex and lead to non-positive Boltzmann weights for the lattice model, a non-Hermitian XX Hamiltonian and a non-unitary CFT. So, on this basis, it could be argued that our dimer model is ‘unphysical’. In fact, our dimer model is just the free-fermion point of the $U_q(\mathfrak{sl}(2))$ -invariant XXZ Hamiltonian [55] which is a *standard* and very well-studied quantum chain. While the $U_q(\mathfrak{sl}(2))$ -invariant XX Hamiltonian is non-Hermitian, its eigenvalues are all real. We have also demonstrated that it exhibits proper conformal properties in the continuum scaling limit. We thus argue that our dimer model on the strip and the $U_q(\mathfrak{sl}(2))$ -invariant XX Hamiltonian should not be regarded as ‘unphysical’ inasmuch as they relate to a seemingly well-defined, albeit logarithmic, CFT. The situation is analogous to the two-dimensional RSOS(2,5) lattice model studied by Forrester and Baxter [56]. Indeed, it could similarly be argued that this model is ‘unphysical’ in the sense that its Boltzmann weights are non-positive, its associated quantum Hamiltonian $\mathcal{H}_{2,5}$ is non-Hermitian and its associated CFT, which is the Yang–Lee minimal model $\mathcal{M}(2, 5)$, is nonunitary. Nevertheless, the free energy, correlation length, local height probabilities and critical exponents of RSOS(2,5) all seem to make good sense. Indeed, for the Ising model in a complex magnetic field, the RSOS(2,5) theory describes [57, 58] the critical behaviour associated with the closure of the Yang–Lee zeros on the unit circle. This Yang–Lee edge singularity exemplifies the Yang–Lee universality class. Although $\mathcal{H}_{2,5}$ is non-Hermitian, its eigenvalues are all real and it provides a good example of

non-Hermitian quantum mechanics [59–61] which is now accepted to have many ‘physical’ applications. Similarly, although it is nonunitary, the minimal model $\mathcal{M}(2, 5)$ is a perfectly well-defined rational CFT [62, 63].

Acknowledgments

JR was supported by the Australian Research Council under the Discovery Project scheme, Project Number DP160101376. AVO is supported by a Melbourne International Research Scholarship and a Melbourne International Fee Remission Scholarship. Parts of this work were carried out while PAP was visiting the APCTP, Pohang, Korea as an ICTP Visiting Scholar. The authors thank Alexi Morin-Duchesne and the referee for helpful comments.

Appendix A. Proof of inversion identities on the strip

In this appendix, we prove the inversion identity (4.1) for dimers on the strip

$$\mathbf{D}(u)\mathbf{D}(u + \lambda) = -\tan^2 2u (\cos^{2N} u - \sin^{2N} u)^2 \mathbf{I}, \quad w = 0 \tag{A.1}$$

where $\mathbf{D}(u)$ is the double row transfer matrix (3.25) with $w = 0$. The inversion identity (4.2) is proved similarly. Throughout this section, we work in the Temperley–Lieb representation with the gauge $g = z := e^{iu}$.

For a column at position j with fixed $a_j, b_j = 0, 1$, let us define the four 16×16 matrices

$$R \begin{pmatrix} a_j \\ b_j \end{pmatrix} = \begin{array}{c} a_j \\ \begin{array}{|c|c|c|} \hline c & u+\lambda & c' \\ \hline d & u+\lambda & d' \\ \hline e & u & e' \\ \hline f & u & f' \\ \hline \end{array} \\ b_j \end{array} . \tag{A.2}$$

The matrix elements of the product of double row transfer matrices, with upper and lower particle state configurations $\mathbf{a} = \{a_1, a_2, \dots, a_N\}$ and $\mathbf{b} = \{b_1, b_2, \dots, b_N\}$, are then given by

$$[\mathbf{D}(u)\mathbf{D}(u + \lambda)]_{\mathbf{b}, \mathbf{a}} = \langle \text{left} | \prod_{j=1}^N R \begin{pmatrix} a_j \\ b_j \end{pmatrix} | \text{right} \rangle, \quad a_j, b_j = 0, 1 \tag{A.3}$$

where the left and right boundary vectors are

$$\langle \text{left} | = (-1, 1, 1, -1, 0, 0, 0, 0, 0, 0, 0, 0, 0, 0, 0, 0) \in \mathcal{V}_6 \tag{A.4}$$

$$| \text{right} \rangle = (1, 1, 1, 1, 0, 0, 0, 0, 0, 0, 0, 0, 0, 0, 0, 0)^T \in \mathcal{V}_6. \tag{A.5}$$

Setting

$$s = \sin u, \quad c = \cos u, \quad z = e^{iu}, \quad x = i \tag{A.6}$$

and ordering the sixteen intermediate basis states as

$$\begin{pmatrix} 0 \\ 0 \\ 0 \\ 0 \end{pmatrix}, \begin{pmatrix} 0 \\ 0 \\ 1 \\ 1 \end{pmatrix}, \begin{pmatrix} 1 \\ 1 \\ 0 \\ 0 \end{pmatrix}, \begin{pmatrix} 1 \\ 1 \\ 1 \\ 1 \end{pmatrix}, \begin{pmatrix} 0 \\ 1 \\ 1 \\ 0 \end{pmatrix}, \begin{pmatrix} 1 \\ 0 \\ 0 \\ 1 \end{pmatrix}; \begin{pmatrix} 0 \\ 0 \\ 0 \\ 1 \end{pmatrix}, \begin{pmatrix} 0 \\ 0 \\ 1 \\ 0 \end{pmatrix}, \begin{pmatrix} 0 \\ 1 \\ 0 \\ 0 \end{pmatrix}, \begin{pmatrix} 0 \\ 1 \\ 1 \\ 0 \end{pmatrix}, \begin{pmatrix} 0 \\ 0 \\ 1 \\ 1 \end{pmatrix}, \begin{pmatrix} 1 \\ 0 \\ 0 \\ 0 \end{pmatrix}, \begin{pmatrix} 1 \\ 0 \\ 1 \\ 1 \end{pmatrix}, \begin{pmatrix} 1 \\ 1 \\ 0 \\ 1 \end{pmatrix}, \begin{pmatrix} 1 \\ 1 \\ 0 \\ 0 \end{pmatrix} \tag{A.7}$$

the four $R^{(a_j)}_{(b_j)}$ matrices are given explicitly by

$$R^{(0)}_{(0)} = \begin{pmatrix} c^2s^2 & 0 & 0 & 0 & \frac{ics}{z^2} & 0 & 0 & 0 & 0 & 0 & 0 & 0 & 0 & 0 & 0 & 0 \\ s^2z^2 & s^4 & 0 & 0 & ics & 0 & 0 & 0 & 0 & 0 & 0 & 0 & 0 & 0 & 0 & 0 \\ -c^2z^2 & 0 & c^4 & 0 & -ics & 0 & 0 & 0 & 0 & 0 & 0 & 0 & 0 & 0 & 0 & 0 \\ -z^4 & -s^2z^2 & c^2z^2 & c^2s^2 & -icsz^2 & 0 & 0 & 0 & 0 & 0 & 0 & 0 & 0 & 0 & 0 & 0 \\ 0 & 0 & 0 & 0 & -c^2s^2 & 0 & 0 & 0 & 0 & 0 & 0 & 0 & 0 & 0 & 0 & 0 \\ icsz^2 & ics & -ics & -\frac{ics}{z^2} & 0 & -c^2s^2 & 0 & 0 & 0 & 0 & 0 & 0 & 0 & 0 & 0 & 0 \\ 0 & 0 & 0 & 0 & 0 & 0 & cs^3 & 0 & is^2 & 0 & \frac{is^2}{z^2} & 0 & 0 & 0 & 0 & 0 \\ 0 & 0 & 0 & 0 & 0 & 0 & 0 & cs^3 & 0 & 0 & 0 & 0 & 0 & 0 & 0 & 0 \\ 0 & 0 & 0 & 0 & 0 & 0 & 0 & 0 & -c^3s & 0 & 0 & 0 & 0 & 0 & 0 & 0 \\ 0 & 0 & 0 & 0 & 0 & 0 & 0 & 0 & 0 & -c^2s^2 & 0 & 0 & 0 & 0 & 0 & 0 \\ 0 & 0 & 0 & 0 & 0 & 0 & 0 & 0 & -csz^2 & 0 & -cs^3 & 0 & 0 & 0 & 0 & 0 \\ 0 & 0 & 0 & 0 & 0 & 0 & 0 & ic^2 & 0 & 0 & 0 & -c^3s & 0 & 0 & 0 & -\frac{ic^2}{z^2} \\ 0 & 0 & 0 & 0 & 0 & 0 & 0 & 0 & 0 & 0 & 0 & 0 & -c^2s^2 & 0 & 0 & 0 \\ 0 & 0 & 0 & 0 & 0 & 0 & 0 & ic^2z^2 & 0 & 0 & 0 & -csz^2 & 0 & -cs^3 & 0 & -ic^2 \\ 0 & 0 & 0 & 0 & 0 & 0 & -csz^2 & 0 & -is^2z^2 & 0 & -is^2 & 0 & 0 & 0 & c^3s & 0 \\ 0 & 0 & 0 & 0 & 0 & 0 & 0 & -csz^2 & 0 & 0 & 0 & 0 & 0 & 0 & 0 & c^3s \end{pmatrix} \tag{A.8}$$

$$R^{(1)}_{(1)} = \begin{pmatrix} c^2s^2 & \frac{c^2}{z^2} & -\frac{s^2}{z^2} & -\frac{1}{z^4} & 0 & \frac{ics}{z^2} & 0 & 0 & 0 & 0 & 0 & 0 & 0 & 0 & 0 & 0 \\ 0 & c^4 & 0 & -\frac{c^2}{z^2} & 0 & ics & 0 & 0 & 0 & 0 & 0 & 0 & 0 & 0 & 0 & 0 \\ 0 & 0 & s^4 & -\frac{s^2}{z^2} & 0 & -ics & 0 & 0 & 0 & 0 & 0 & 0 & 0 & 0 & 0 & 0 \\ 0 & 0 & 0 & \frac{c^2}{z^2} & c^2s^2 & -icsz^2 & 0 & 0 & 0 & 0 & 0 & 0 & 0 & 0 & 0 & 0 \\ icsz^2 & ics & -ics & -\frac{ics}{z^2} & -c^2s^2 & 0 & 0 & 0 & 0 & 0 & 0 & 0 & 0 & 0 & 0 & 0 \\ 0 & 0 & 0 & 0 & 0 & -c^2s^2 & 0 & 0 & 0 & 0 & 0 & 0 & 0 & 0 & 0 & 0 \\ 0 & 0 & 0 & 0 & 0 & 0 & c^3s & 0 & 0 & 0 & 0 & 0 & 0 & 0 & 0 & -\frac{ics}{z^2} \\ 0 & 0 & 0 & 0 & 0 & 0 & 0 & c^3s & 0 & 0 & is^2 & 0 & \frac{is^2}{z^2} & 0 & 0 & -\frac{cs}{z^2} \\ 0 & 0 & 0 & 0 & 0 & 0 & ic^2 & 0 & -cs^3 & 0 & -\frac{cs}{z^2} & 0 & 0 & 0 & -\frac{ic^2}{z^2} & 0 \\ 0 & 0 & 0 & 0 & 0 & 0 & 0 & 0 & 0 & -c^2s^2 & 0 & 0 & 0 & 0 & 0 & 0 \\ 0 & 0 & 0 & 0 & 0 & 0 & ic^2z^2 & 0 & 0 & 0 & -c^3s & 0 & 0 & 0 & 0 & -ic^2 \\ 0 & 0 & 0 & 0 & 0 & 0 & 0 & 0 & 0 & 0 & -cs^3 & 0 & -\frac{cs}{z^2} & 0 & 0 & 0 \\ 0 & 0 & 0 & 0 & 0 & 0 & 0 & 0 & 0 & 0 & 0 & -c^2s^2 & 0 & 0 & 0 & 0 \\ 0 & 0 & 0 & 0 & 0 & 0 & 0 & 0 & 0 & 0 & 0 & 0 & 0 & -c^3s & 0 & 0 \\ 0 & 0 & 0 & 0 & 0 & 0 & 0 & 0 & 0 & 0 & 0 & 0 & 0 & 0 & cs^3 & 0 \\ 0 & 0 & 0 & 0 & 0 & 0 & 0 & 0 & 0 & 0 & -is^2z^2 & 0 & -is^2 & 0 & 0 & cs^3 \end{pmatrix} \tag{A.9}$$

$$R^{(0)}_{(1)} = \begin{pmatrix} 0 & 0 & 0 & 0 & 0 & 0 & \frac{cs^2}{z} & 0 & \frac{is^3}{z} & 0 & \frac{is}{z^3} & 0 & 0 & 0 & 0 & 0 \\ 0 & 0 & 0 & 0 & 0 & 0 & cs^2z & 0 & 0 & 0 & \frac{ic^2s}{z} & 0 & 0 & 0 & 0 & 0 \\ 0 & 0 & 0 & 0 & 0 & 0 & -cz & 0 & -is^3z & 0 & -\frac{is}{z} & 0 & 0 & 0 & 0 & \frac{c^3}{z} \\ 0 & 0 & 0 & 0 & 0 & 0 & -cz^3 & 0 & 0 & 0 & -ic^2sz & 0 & 0 & 0 & 0 & c^3z \\ 0 & 0 & 0 & 0 & 0 & 0 & 0 & 0 & -cs^2z & 0 & -\frac{cs^2}{z} & 0 & 0 & 0 & 0 & 0 \\ 0 & 0 & 0 & 0 & 0 & 0 & ic^2sz & 0 & 0 & 0 & 0 & 0 & 0 & 0 & 0 & -\frac{ic^2s}{z} \\ 0 & 0 & 0 & 0 & 0 & 0 & 0 & 0 & 0 & \frac{ics^2}{z} & 0 & 0 & 0 & 0 & 0 & 0 \\ s^3z & \frac{s^3}{z} & 0 & 0 & \frac{ics^2}{z} & 0 & 0 & 0 & 0 & 0 & 0 & 0 & 0 & 0 & 0 & 0 \\ 0 & 0 & 0 & 0 & 0 & 0 & 0 & 0 & 0 & -\frac{c^2s}{z} & 0 & 0 & 0 & 0 & 0 & 0 \\ 0 & 0 & 0 & 0 & 0 & 0 & 0 & 0 & 0 & 0 & 0 & 0 & 0 & 0 & 0 & 0 \\ 0 & 0 & 0 & 0 & 0 & 0 & 0 & 0 & 0 & -c^2sz & 0 & 0 & 0 & 0 & 0 & 0 \\ ics^2z & \frac{ic}{z} & -\frac{ics^2}{z} & -\frac{ic}{z^3} & 0 & -\frac{c^2s}{z} & 0 & 0 & 0 & 0 & 0 & 0 & 0 & 0 & 0 & 0 \\ 0 & 0 & 0 & 0 & 0 & 0 & 0 & ic^2sz & 0 & 0 & 0 & -cs^2z & 0 & -\frac{cs^2}{z} & 0 & -\frac{ic^2s}{z} \\ 0 & ic^3z & 0 & -\frac{ic^3}{z} & 0 & -c^2sz & 0 & 0 & 0 & 0 & 0 & 0 & 0 & 0 & 0 & 0 \\ 0 & 0 & 0 & 0 & 0 & 0 & 0 & 0 & 0 & 0 & -ics^2z & 0 & 0 & 0 & 0 & 0 \\ -sz^3 & -sz & c^2sz & \frac{c^2s}{z} & -ics^2z & 0 & 0 & 0 & 0 & 0 & 0 & 0 & 0 & 0 & 0 & 0 \end{pmatrix} \tag{A.10}$$

J. Stat. Mech. (2020) 013107

$$R\begin{pmatrix} 1 \\ 0 \end{pmatrix} = \begin{pmatrix} 0 & 0 & 0 & 0 & 0 & 0 & 0 & \frac{c^3}{z} & 0 & 0 & 0 & \frac{ic^2s}{z} & 0 & 0 & 0 & -\frac{cs^3}{z^3} \\ 0 & 0 & 0 & 0 & 0 & 0 & 0 & c^3z & 0 & 0 & 0 & isz & 0 & \frac{is^3}{z} & 0 & -\frac{ics}{z^3} \\ 0 & 0 & 0 & 0 & 0 & 0 & 0 & 0 & 0 & 0 & 0 & -ic^2sz & 0 & 0 & 0 & \frac{cs^2}{z} \\ 0 & 0 & 0 & 0 & 0 & 0 & 0 & 0 & 0 & 0 & 0 & -is^3z & 0 & -is^3z & 0 & \frac{cs^2z}{z} \\ 0 & 0 & 0 & 0 & 0 & 0 & 0 & ic^2sz & 0 & 0 & 0 & 0 & 0 & 0 & 0 & -\frac{ic^2s}{z} \\ 0 & 0 & 0 & 0 & 0 & 0 & 0 & 0 & 0 & 0 & 0 & -cs^2z & 0 & -\frac{cs^2}{z} & 0 & 0 \\ c^2sz & \frac{c^2s}{z} & -\frac{cs^3}{z} & -\frac{s}{z^3} & 0 & \frac{ics^2}{z} & 0 & 0 & 0 & 0 & 0 & 0 & 0 & 0 & 0 & 0 \\ 0 & 0 & 0 & 0 & 0 & 0 & 0 & 0 & 0 & 0 & 0 & 0 & \frac{ics^2}{z} & 0 & 0 & 0 \\ ic^3z & 0 & -\frac{ic^3}{z} & 0 & -\frac{c^2s}{z} & 0 & 0 & 0 & 0 & 0 & 0 & 0 & 0 & 0 & 0 & 0 \\ 0 & 0 & 0 & 0 & 0 & 0 & ic^2sz & 0 & -cs^2z & 0 & -\frac{cs^2}{z} & 0 & 0 & 0 & -\frac{ic^2s}{z} & 0 \\ icz^3 & ics^2z & -icz & -\frac{ics^2}{z} & -c^2sz & 0 & 0 & 0 & 0 & 0 & 0 & 0 & 0 & 0 & 0 & 0 \\ 0 & 0 & 0 & 0 & 0 & 0 & 0 & 0 & 0 & 0 & 0 & 0 & -\frac{c^2s}{z} & 0 & 0 & 0 \\ 0 & 0 & 0 & 0 & 0 & 0 & 0 & 0 & 0 & 0 & 0 & 0 & 0 & 0 & 0 & 0 \\ 0 & 0 & 0 & 0 & 0 & 0 & 0 & 0 & 0 & 0 & 0 & 0 & -c^2sz & 0 & 0 & 0 \\ 0 & 0 & s^3z & \frac{s^3}{z} & 0 & -ics^2z & 0 & 0 & 0 & 0 & 0 & 0 & 0 & 0 & 0 & 0 \\ 0 & 0 & 0 & 0 & 0 & 0 & 0 & 0 & 0 & 0 & 0 & 0 & -ics^2z & 0 & 0 & 0 \end{pmatrix}. \tag{A.11}$$

The matrices $R\begin{pmatrix} 0 \\ 0 \end{pmatrix}$ and $R\begin{pmatrix} 1 \\ 1 \end{pmatrix}$ are block diagonal under a direct sum decomposition of the intermediate basis of states

$$\mathcal{V} = \mathcal{V}_6 \oplus \mathcal{V}_{10} \tag{A.12}$$

so that

$$R\begin{pmatrix} a \\ a \end{pmatrix} : \quad \mathcal{V}_6 \rightarrow \mathcal{V}_6, \quad \mathcal{V}_{10} \rightarrow \mathcal{V}_{10}. \tag{A.13}$$

We show that non-diagonal matrix elements with $\mathbf{a} \neq \mathbf{b}$ vanish. In this case, the states on the left and right in (A.3) are built up by the action of $R\begin{pmatrix} a \\ b \end{pmatrix}$ on the left and right boundaries $\langle \text{left} |$ and $|\text{right}\rangle$ with the occurrence of at least one $R\begin{pmatrix} a \\ 1-a \end{pmatrix}$ matrix. We begin building up the states by acting with $R\begin{pmatrix} a \\ a \end{pmatrix}$ on the left and right states. We find that

$$v_{\text{left}} = \langle \text{left} | \prod_{j=0}^n R\begin{pmatrix} a_j \\ a_j \end{pmatrix} \in \mathcal{V}_{\text{left}}, \quad v_{\text{right}} = \prod_{j=0}^n R\begin{pmatrix} a_j \\ a_j \end{pmatrix} |\text{right}\rangle \in \mathcal{V}_{\text{right}}, \quad n \geq 0 \tag{A.14}$$

where the vector spaces $\mathcal{V}_{\text{left}}, \mathcal{V}_{\text{right}}$ are given by the linear spans

$$\mathcal{V}_{\text{left}} = \left\langle \left\{ \langle \text{left} |, \langle \text{left} | R\begin{pmatrix} 0 \\ 0 \end{pmatrix}, \langle \text{left} | R\begin{pmatrix} 1 \\ 1 \end{pmatrix}, \langle \text{left} | R\begin{pmatrix} 0 \\ 0 \end{pmatrix}^2 \right\} \right\rangle \tag{A.15}$$

$$\mathcal{V}_{\text{right}} = \left\langle \left\{ |\text{right}\rangle, R\begin{pmatrix} 0 \\ 0 \end{pmatrix} |\text{right}\rangle, R\begin{pmatrix} 1 \\ 1 \end{pmatrix} |\text{right}\rangle, R\begin{pmatrix} 0 \\ 0 \end{pmatrix}^2 |\text{right}\rangle \right\} \right\rangle. \tag{A.16}$$

These spaces are stable under the action of further $R\begin{pmatrix} a \\ a \end{pmatrix}$ matrices. The linear independence of vectors is easily checked by calculating the rank of suitable matrices in Mathematica [38]. Since

$$v_{\text{left}} R\begin{pmatrix} a \\ 1-a \end{pmatrix} v_{\text{right}} = 0 \tag{A.17}$$

let assume next that there are at least two $R\begin{pmatrix} a \\ 1-a \end{pmatrix}$ matrices. In this case, we similarly find that

$$v'_{\text{left}} = v_{\text{left}} R\begin{pmatrix} a \\ 1-a \end{pmatrix} \prod_{j=0}^n R\begin{pmatrix} a_j \\ a_j \end{pmatrix} \in \left\langle \left\{ \langle \text{left} | R\begin{pmatrix} a \\ 1-a \end{pmatrix}, \langle \text{left} | R\begin{pmatrix} 0 \\ 0 \end{pmatrix} R\begin{pmatrix} a \\ 1-a \end{pmatrix} \right\} \right\rangle = \mathcal{V}'_{\text{left}}, \quad n \geq 0 \tag{A.18}$$

$$v'_{\text{right}} = \prod_{j=0}^n R\left(\begin{smallmatrix} a_j \\ a_j \end{smallmatrix}\right) R\left(\begin{smallmatrix} a \\ 1-a \end{smallmatrix}\right) v_{\text{right}} \in \langle \{R\left(\begin{smallmatrix} a \\ 1-a \end{smallmatrix}\right) |_{\text{right}}, R\left(\begin{smallmatrix} a \\ 1-a \end{smallmatrix}\right) R\left(\begin{smallmatrix} 0 \\ 0 \end{smallmatrix}\right) |_{\text{right}}\} \rangle = \mathcal{V}'_{\text{right}}, \quad n \geq 0 \tag{A.19}$$

where the vector spaces are orthogonal. So next suppose that there are three or more $R\left(\begin{smallmatrix} a \\ 1-a \end{smallmatrix}\right)$ matrices. In this case, we observe that

$$v_{\text{left}} R\left(\begin{smallmatrix} a \\ 1-a \end{smallmatrix}\right) \prod_{j=0}^n R\left(\begin{smallmatrix} a_j \\ a_j \end{smallmatrix}\right) R\left(\begin{smallmatrix} a \\ 1-a \end{smallmatrix}\right) = R\left(\begin{smallmatrix} a \\ 1-a \end{smallmatrix}\right) \prod_{j=0}^n R\left(\begin{smallmatrix} a_j \\ a_j \end{smallmatrix}\right) R\left(\begin{smallmatrix} a \\ 1-a \end{smallmatrix}\right) v_{\text{right}} = \mathbf{0} \tag{A.20}$$

so that the occurrence of the matrices $R\left(\begin{smallmatrix} 0 \\ 1 \end{smallmatrix}\right)$ and $R\left(\begin{smallmatrix} 1 \\ 0 \end{smallmatrix}\right)$ must alternate along the segment. Moreover, we observe that

$$v_{\text{left}}^{\text{eig}} = v'_{\text{left}} R\left(\begin{smallmatrix} a \\ 1-a \end{smallmatrix}\right) R\left(\begin{smallmatrix} 1-a \\ a \end{smallmatrix}\right), \quad v'_{\text{left}} \in \mathcal{V}'_{\text{left}}, \quad v_{\text{right}}^{\text{eig}} = R\left(\begin{smallmatrix} a \\ 1-a \end{smallmatrix}\right) R\left(\begin{smallmatrix} 1-a \\ a \end{smallmatrix}\right) v'_{\text{right}}, \quad v'_{\text{right}} \in \mathcal{V}'_{\text{right}} \tag{A.21}$$

are simultaneous (respectively left and right) eigenvectors of $R\left(\begin{smallmatrix} 0 \\ 0 \end{smallmatrix}\right)$ and $R\left(\begin{smallmatrix} 1 \\ 1 \end{smallmatrix}\right)$ satisfying the orthogonality

$$v_{\text{left}}^{\text{eig}} \cdot v_{\text{right}}^{\text{eig}} = 0, \quad v_{\text{left}}^{\text{eig}} R\left(\begin{smallmatrix} a \\ 1-a \end{smallmatrix}\right) = \mathbf{0}, \quad R\left(\begin{smallmatrix} a \\ 1-a \end{smallmatrix}\right) v_{\text{right}}^{\text{eig}} = \mathbf{0}. \tag{A.22}$$

It follows that the only nonzero matrix elements in (A.3) are diagonal with $\mathbf{a} = \mathbf{b}$ and

$$[\mathbf{D}(u)\mathbf{D}(u+\lambda)]_{\mathbf{a},\mathbf{a}} = {}_6\langle \text{left} | \prod_{j=1}^N R\left(\begin{smallmatrix} a_j \\ a_j \end{smallmatrix}\right) |_{\text{right}} \rangle_6, \quad a_j = 0, 1 \tag{A.23}$$

where $R\left(\begin{smallmatrix} a \\ a \end{smallmatrix}\right)_6$ denotes the 6×6 diagonal block of $R\left(\begin{smallmatrix} a \\ a \end{smallmatrix}\right)$ and

$${}_6\langle \text{left} | = (-1, 1, 1, -1, 0, 0), \quad |_{\text{right}} \rangle_6 = (1, 1, 1, 1, 0, 0)^T. \tag{A.24}$$

Let us now suppose that $\mathbf{a} = \mathbf{b} = (0, 0, 0, \dots, 0, 0)$ and observe that $R\left(\begin{smallmatrix} 0 \\ 0 \end{smallmatrix}\right)$ can be diagonalized by a similarity transformation

$$S^{-1} R\left(\begin{smallmatrix} 0 \\ 0 \end{smallmatrix}\right) S = \begin{pmatrix} s^4 & 0 & 0 & 0 & 0 & 0 \\ 0 & c^4 & 0 & 0 & 0 & 0 \\ 0 & 0 & s^2 c^2 & 0 & 0 & 0 \\ 0 & 0 & 0 & s^2 c^2 & 0 & 0 \\ 0 & 0 & 0 & 0 & -s^2 c^2 & 0 \\ 0 & 0 & 0 & 0 & 0 & -s^2 c^2 \end{pmatrix}, \tag{A.25}$$

$$S = \begin{pmatrix} 0 & 0 & -\frac{(z^4-1)^2(z^4+1)}{4z^8} & \frac{z^8-1}{2z^8} & 0 & \frac{z^4+1}{z^4} \\ -\frac{(z^4+1)^2}{2z^4} & 0 & -\frac{(z^4-1)^2}{2z^4} & \frac{z^4-1}{z^4} & 0 & \frac{(z^4+1)^2}{2z^4} \\ 0 & -\frac{(z^4+1)^2}{2z^4} & -\frac{(z^4-1)^2}{2z^4} & \frac{z^4-1}{z^4} & 0 & \frac{(z^4+1)^2}{2z^4} \\ -z^4-1 & -z^4-1 & 0 & \frac{z^8-1}{2z^4} & 0 & z^4+1 \\ 0 & 0 & 0 & 0 & 0 & \frac{z^8-1}{2z^4} \\ \frac{z^8-1}{2z^4} & \frac{z^8-1}{2z^4} & \frac{z^8-1}{2z^4} & 0 & \frac{z^8-1}{2z^4} & 0 \end{pmatrix}$$

J. Stat. Mech. (2020) 013107

with

$${}_6\langle\text{left}|S = \left(\frac{z^8 - 1}{2z^4}, \frac{z^8 - 1}{2z^4}, -\frac{(z^4 - 1)^2(3z^4 - 1)}{4z^8}, -\frac{(z^4 - 1)^3}{2z^8}, 0, 0\right) \tag{A.26}$$

$$S^{-1}|\text{right}\rangle_6 = \left(\frac{2z^4(z^4 - 1)}{(z^4 + 1)^3}, \frac{2z^4(z^4 - 1)}{(z^4 + 1)^3}, -\frac{4z^4(z^4 - 1)}{(z^4 + 1)^3}, \frac{2z^4(5z^8 - 2z^4 + 1)}{(z^4 - 1)(z^4 + 1)^3}, 0, 0\right). \tag{A.27}$$

Putting everything together, it follows that

$${}_6\langle\text{left}|R\binom{0}{0}\rangle_6^N |\text{right}\rangle_6 = -\tan^2 2u [c^{4N} - 2(sc)^{2N} + s^{4N}] = -\tan^2 2u [c^{2N} - s^{2N}]^2. \tag{A.28}$$

The last step is to extend this result to all the other diagonal segments. To do this let us define

$$\Delta R = \frac{2z^2}{1 - z^4} \left[R\binom{0}{0} - R\binom{1}{1} \right]. \tag{A.29}$$

We then find, using induction, that

$$\prod_{j=1}^{N-1} R\binom{a_j}{a_j} \Delta R |\text{right}\rangle_6 = (-s^2c^2)^{N-1} (z^{-2}, \cos 2u, \cos 2u, z^2, i \sin 2u, i \sin 2u)^T, \quad a_j = 0, 1. \tag{A.30}$$

It follows that

$${}_6\langle\text{left}| \prod_{j=1}^{N-1} R\binom{a_j}{a_j} \Delta R |\text{right}\rangle_6 = 0. \tag{A.31}$$

So the weight of the diagonal matrix elements with $\mathbf{b} = \mathbf{a}$ are independent of \mathbf{a}

$$[\mathbf{D}(u)\mathbf{D}(u + \lambda)]_{\mathbf{a},\mathbf{a}} = {}_6\langle\text{left}| \prod_{j=1}^N R\binom{a_j}{a_j} |\text{right}\rangle_6 = -\tan^2 2u [c^{2N} - s^{2N}]^2. \tag{A.32}$$

Appendix B. Skew q -binomials

The skew q -binomials, related to generalized q -Narayana numbers (4.15), are [31, 32]

$$\begin{aligned} \left\{ \begin{matrix} M \\ m, n \end{matrix} \right\}_q &= \begin{bmatrix} M \\ m \end{bmatrix} \begin{bmatrix} M \\ n \end{bmatrix} - q^{n-m+1} \begin{bmatrix} M \\ m-1 \end{bmatrix} \begin{bmatrix} M \\ n+1 \end{bmatrix} \\ &= q^{-M+n} \left(\begin{bmatrix} M \\ m \end{bmatrix} \begin{bmatrix} M+1 \\ n+1 \end{bmatrix} - \begin{bmatrix} M+1 \\ m \end{bmatrix} \begin{bmatrix} M \\ n+1 \end{bmatrix} \right), \quad 0 \leq m \leq n \leq M. \end{aligned} \tag{B.1}$$

At $q = 1$, the skew binomials $\left\{ \begin{matrix} M \\ m, m \end{matrix} \right\}_{q=1}$ are determinants of ordinary binomials

Binomials	Skew Binomials ($n = m$)	Catalan	
1	1	1	
1 1	1 1	2	
1 2 1	1 3 1	5	(B.2)
1 3 3 1	1 6 6 1	14	
1 4 6 4 1	1 10 20 10 1	42	
1 5 10 10 5 1	1 15 50 50 15 1	132	

The skew q -binomials are enumerated by double column diagrams with dominance

$$1 + 2q + 2q^2 + 2q^3 + q^4 = \left\{ \begin{matrix} 3 \\ 1, 2 \end{matrix} \right\}_q \quad (B.3)$$

A partition λ is equivalent to a Young diagram Y . A skew Young diagram Y_2/Y_1 is equivalent to the pair (Y_1, Y_2) with $Y_1 \subseteq Y_2$. Let us define

$$E(Y) = \text{Energy} = \{\# \text{ of boxes in the Young diagram } Y\} \quad (B.4)$$

$$Y_{m,n} = \{m \times n \text{ rectangular Young diagram}\}$$

A skew q -binomial can be written as an energy weighted sum over skew Young diagrams

$$\left\{ \begin{matrix} M \\ m, n \end{matrix} \right\}_q = q^{(m-n)n} \sum_{\substack{Y_1 \subseteq Y_2 \\ \emptyset \subseteq Y_1 \subseteq Y_{M-m,m} \\ Y_{n-m,n} \subseteq Y_2 \subseteq Y_{M-m,n}}} q^{E(Y_1)+E(Y_2)}, \quad 0 \leq m \leq n \leq M. \quad (B.5)$$

The bijection is implemented by interpreting the left and right column (particle) configurations in the double column diagrams as Maya diagrams and using the standard bijection between Maya diagrams and Young diagrams. For example, shading Y_1 , gives

$$\left\{ \begin{matrix} 3 \\ 1, 2 \end{matrix} \right\}_q = q^{-2} \left[1 + 2q + 2q^2 + 2q^3 + q^4 \right], \quad \begin{matrix} \emptyset \subseteq Y_1 \subseteq Y_{2,1} \\ Y_{1,2} \subseteq Y_2 \subseteq Y_{2,2} \end{matrix} \quad (B.6)$$

References

- [1] Roberts J K 1935 Some properties of adsorbed films of oxygen on tungsten *Proc. R. Soc. A* **152** 464–77
- [2] Fowler R H and Rushbrooke G S 1937 An attempt to extend the statistical theory of perfect solutions *Trans. Faraday Soc.* **33** 1272–94

- [3] Kasteleyn P W 1961 The statistics of dimers on a lattice: I. The number of dimer arrangements on a quadratic lattice *Physica* **27** 1209–25
- Kasteleyn P W 1963 Dimer statistics and phase transitions *J. Math. Phys.* **4** 287–93
- [4] Temperley H N V and Fisher M E 1961 Dimer problem in statistical mechanics—an exact result *Phil. Mag.* **6** 1061–3
- [5] Fisher M E 1961 Statistical mechanics of dimers on a plane lattice *Phys. Rev.* **124** 1664–72
- [6] Lieb E H 1967 Solution of the dimer problem by the transfer matrix method *J. Math. Phys.* **8** 2339–41
- [7] Izmailian N Sh, Oganesyanyan K B and Hu C-K 2003 Exact finite-size corrections of the free energy for the square lattice dimer model under different boundary conditions *Phys. Rev. E* **67** 066114
- [8] Izmailian N Sh, Priezzhev V B, Ruelle P and Hu C-K 2005 Logarithmic conformal field theory and boundary effects in the dimer model *Phys. Rev. Lett.* **95** 260602
- [9] Izmailian N Sh, Priezzhev V B and Ruelle P 2007 Non-local finite-size effects in the dimer model *Symmetry Integr. Geom.* **3** 001
- [10] Rasmussen J and Ruelle P 2012 Refined conformal spectra in the dimer model *J. Stat. Mech.* P10002
- [11] Nigro A 2012 Finite size corrections for dimers (arXiv:1208.2110 [math-ph])
- [12] Allegra N 2015 Exact solution of the 2D dimer model: Corner free energy, correlation functions and combinatorics *Nucl. Phys. B* **894** 685–732
- [13] Morin-Duchesne A, Rasmussen J and Ruelle P 2015 Dimer representations of the Temperley–Lieb algebra *Nucl. Phys. B* **890** 363–87
- [14] Morin-Duchesne A, Rasmussen J and Ruelle P 2016 Integrability and conformal data of the dimer model *J. Phys. A: Math. Theor.* **49** 174002
- [15] Elkies N, Kuperberg G, Larsen M and Propp J 1992 Alternating-sign matrices and domino tilings (Part I) *J. Algebr. Comb.* **1** 111–32
- Elkies N, Kuperberg G, Larsen M and Propp J 1992 Alternating-sign matrices and domino tilings (Part II) *J. Algebr. Comb.* **1** 219–34
- [16] Korepin V E 1982 Calculation of norms of Bethe wave functions *Commun. Math. Phys.* **86** 391–418
- [17] Korepin V and Zinn-Justin P 2000 Thermodynamic limit of the six-vertex model with domain wall boundary conditions *J. Phys. A: Math. Theor.* **33** 7053
- [18] Kenyon R 2000 Conformal invariance of domino tiling *Ann. Probab.* **28** 759–95
- Kenyon R 2001 Dominoes and the Gaussian free field *Ann. Probab.* **29** 1128–37
- Kenyon R 2009 Lectures on dimers (arXiv:0910.3129)
- [19] Pearce P A and Vittorini-Orgeas A 2017 Yang–Baxter solution of dimers as a free-fermion six-vertex model *J. Phys. A: Math. Theor.* **50** 434001
- [20] Baxter R J 1982 *Exactly Solved Models in Statistical Mechanics* (London: Academic)
- [21] Baxter R J 1972 Partition function of the eight-vertex model *Ann. Phys., NY* **70** 193–228 (appendix A)
- [22] Ferrari P L and Spohn H 2006 Domino tilings and the six-vertex model at its free-fermion point *J. Phys. A: Math. Theor.* **39** 10297
- [23] Pauling L 1935 The structure and entropy of ice and of other crystals with some randomness of atomic arrangement *J. Am. Chem. Soc.* **57** 2680–4
- [24] Lieb E H 1967 Residual entropy of square ice *Phys. Rev.* **162** 162–72
- Lieb E H 1967 Exact solution of the F model of an antiferroelectric *Phys. Rev. Lett.* **18** 1046–8
- Lieb E H 1967 Exact solution of the two-dimensional Slater KDP model of a ferroelectric *Phys. Rev. Lett.* **19** 108–10
- [25] Sutherland B 1967 Exact solution of a two-dimensional model for hydrogen-bonded crystals *Phys. Rev. Lett.* **19** 103–4
- [26] Lieb E H and Wu F Y 1972 Two dimensional ferroelectric models *Phase Transitions and Critical Phenomena* vol 1, ed C Domb and M S Green (London: Academic) pp 331–490
- [27] Fan C and Wu F Y 1969 Ising model with second neighbor interaction. I. Some exact results and an approximate solution *Phys. Rev.* **179** 560–70
- Fan C and Wu F Y 1970 General lattice model of phase transitions *Phys. Rev. B* **2** 723–33
- [28] Felderhof B U 1973 Direct diagonalization of the transfer matrix of the zero-field free-fermion model *Physica* **65** 421–51
- [29] O’Brien D L, Pearce P A and Warnaar S O 1996 Finitized conformal spectrum of the Ising model on the cylinder and torus *Physica A* **228** 63–77
- [30] Saleur H 1992 Polymers and percolation in two dimensions and twisted $N = 2$ supersymmetry *Nucl. Phys. B* **382** 486–531
- [31] Pearce P A and Rasmussen J 2007 Solvable critical dense polymers *J. Stat. Mech.* P02015
- [32] Pearce P A and Rasmussen J 2007 Physical combinatorics of critical dense polymers (unpublished)

- [33] Pearce P A, Rasmussen J and Villani S P 2010 Solvable critical dense polymers on the cylinder *J. Stat. Mech.* **P02010**
- [34] Pearce P A, Rasmussen J and Villani S P 2013 Infinitely extended Kac table of solvable critical dense polymers *J. Phys. A: Math. Theor.* **46** 175202
- [35] Morin-Duchesne A, Pearce P A and Rasmussen J 2013 Modular invariant partition function of critical dense polymers *Nucl. Phys. B* **874** 312–57
- [36] Kim D and Pearce P A 1987 Scaling dimensions and conformal anomaly in anisotropic lattice spin model *J. Phys. A: Math. Gen.* **20** L451
- [37] Temperley H N V and Lieb E H 1971 Relations between the ‘percolation’ and ‘colouring’ problem and other graph-theoretical problems associated with regular planar lattices: some exact results for the ‘percolation’ problem *Proc. R. Soc. A* **322** 251–80
- [38] Wolfram Research 2015 *Mathematica Edition: Version 10.0* (Champaign, IL: Wolfram Research Inc.)
- [39] Jones V F R 1994 A quotient of the affine Hecke algebra in the Brauer algebra *L’Enseignement Math.* **40** 313–44
- [40] Jones V F R 1999 Planar algebras I (arXiv:mathQA/9909027)
- [40] Lieb E, Schultz T and Mattis D 1961 Two soluble models of an antiferromagnetic chain *Ann. Phys., NY* **16** 407–66
- [41] Gainutdinov M A, Saleur H and Tipunin I Y 2014 Lattice W -algebras, logarithmic CFTs *J. Phys. A: Math. Theor.* **47** 495401
- [42] Sklyanin E K 1988 Boundary conditions for integrable quantum systems *J. Phys. A: Math. Gen.* **21** 2375–89
- [43] Behrend R E, Pearce P A and O’Brien D L 1996 Interaction-round-a-face models with fixed boundary conditions: the ABF fusion hierarchy *J. Stat. Phys.* **84** 1–48
- [44] Bianchini D, Ercolessi E, Pearce P A and Ravanini F 2015 RSOS quantum chains associated with off-critical minimal models, \mathbb{Z}_n parafermions *J. Stat. Mech.* **P03010**
- [45] Cherednik I V 1984 Factorizing particles on a half-line and root systems *Theor. Math. Phys.* **61** 977–83
- [46] Gaberdiel M R and Kausch H G 1996 A rational logarithmic conformal field theory *Phys. Lett. B* **386** 131–7
- [46] Gaberdiel M R and Kausch H G 1999 A local logarithmic conformal field theory *Nucl. Phys. B* **538** 631–58
- [46] Kausch H G 2000 Symplectic fermions *Nucl. Phys. B* **583** 513–41
- [46] Gaberdiel M R and Runkel I 2008 From boundary to bulk in logarithmic CFT *J. Phys. A: Math. Theor.* **41** 075402
- [47] Morin-Duchesne A 2011 A proof of selection rules for critical dense polymers *J. Phys. A: Math. Theor.* **44** 495003
- [48] Förlinger J and Hofbauer J 1985 q -Catalan numbers *J. Comb. Theory A* **40** 248–64
- [49] Brändén P 2004 q -Narayana numbers and the flag h -vector of $J(2 \times n)$ *Discrete Math.* **281** 67–81
- [50] Morin-Duchesne A, Rasmussen J, Ruelle P and Saint-Aubin Y 2016 On the reality of spectra of $U_q(\mathfrak{sl}(2))$ -invariant XXZ Hamiltonian *J. Stat. Mech.* **053105**
- [51] Gainutdinov A M, Hao W, Nepomechie R I and Sommesse A J 2015 Counting solutions of the Bethe equations of the quantum group invariant open XXZ chain at roots of unity *J. Phys. A: Math. Theor.* **48** 494003
- [52] Gaberdiel M R and Kausch H G 1996 Indecomposable fusion products *Nucl. Phys. B* **477** 293–318
- [53] Rasmussen J 2011 Classification of Kac representations in the logarithmic minimal models $\mathcal{LM}(1, p)$ *Nucl. Phys. B* **853** 404–35
- [54] Feigin B L and Fuchs D B 1982 Invariant skew-symmetric differential operators on the line, Verma modules over the Virasoro algebra *Funct. Anal. Appl.* **16** 114–26
- [54] Iohara K and Koga Y 2011 *Representation Theory of the Virasoro Algebra* (Berlin: Springer)
- [55] Pasquier V and Saleur H 1990 Common structures between finite systems and conformal field theories through quantum groups *Nucl. Phys. B* **330** 523–56
- [56] Forrester P J and Baxter R J 1985 Further exact solutions of the eight-vertex SOS model and generalizations of the Rogers–Ramanujan identities *J. Stat. Phys.* **38** 435–72
- [57] Fisher M E 1978 Yang–Lee edge singularity and ϕ^3 field theory *Phys. Rev. Lett.* **40** 1610–3
- [58] Cardy J L 1985 Conformal invariance and the Yang–Lee edge singularity in two dimensions *Phys. Rev. Lett.* **54** 1354–6
- [59] Bender C M and Boettcher S 1998 Real spectra in non-Hermitian Hamiltonians having PT symmetry *Phys. Rev. Lett.* **80** 5243–6
- [60] Moiseyev N 2011 *Non-Hermitian Quantum Mechanics* (Cambridge: Cambridge University Press)
- [61] Bender C M 2019 *PT Symmetry: in Quantum, Classical Physics* (Singapore: World Scientific)

- [62] Belavin A A, Polyakov A M and Zamolodchikov A B 1984 Infinite conformal symmetry in two-dimensional quantum field theory *Nucl. Phys. B* **241** 333–80
- Belavin A A, Polyakov A M and Zamolodchikov A B 1984 Infinite conformal symmetry of critical fluctuations in two dimensions *J. Stat. Phys.* **34** 763–74
- [63] Bajnok Z, el Deeb O and Pearce P A 2015 Finite-volume spectra of the Lee–Yang model *J. High Energy Phys.* **73**